6-27-2016 12:00 AM

# Electrokinetics and Vacuum Combined Dewatering of Oil Sand Tailings

Rui Zhang, *The University of Western Ontario*

Supervisor: Julie Shang, *The University of Western Ontario*

A thesis submitted in partial fulfillment of the requirements for the Master of Engineering Science degree in Civil and Environmental Engineering

`

# ABSTRACT

One of the challenges faced by the oil sand industry is the dewatering of mature fine oil sands tailings (MFT) due to the low permeability. Vacuum pressure or electrokinetic (EK) dewatering is effective to meet this objective. This research was focused on the experimental study and analytical modelling to explore the influence of combined vacuum and EK treatment on MFT. In this study, systematical experiments on MFT recovered from the northern Alberta were carried out. At first, the characterization and EK cell tests were conducted to measure the basic properties and the coefficient of electroosmotic permeability ($k_e$) of MFT. Secondly, dewatering experiments were carried out with three conditions, i.e. EK dewatering, vacuum pressure dewatering and surcharge preloading dewatering. In this phase of the research, experiments on dewatering by EK combined vacuum pressure treatment and EK combined surcharge preloading treatment were performed in an EK-vacuum cell designed and fabricated for this research. The results of dewatering treatment were assessed with the final water content, undrained shear strength and power consumption etc. Moreover，the theoretical analysis was carried out to examine the feasibility of one dimensional consolidation of MFT based on small strain theory under specific testing conditions. An analytical solution was derived, with variables including the surcharge pressure, vacuum pressure and voltage. The result of the experiments showed the positive effect of dewatering of MFT by EK combined vacuum pressure treatment. After the treatment, the undrained shear strength of MFT

`

reached 5kPa along with significant reduction in water content, which can be as low as 27.7%. The theoretical model based on the small strain theory simulates the consolidate rate well; yet it is not able to accurately predict the final settlements. A further study incorporating the large strain consolidation theory is needed.

*Key words*: electrokinetics, electroosmosis, vacuum and surcharge consolidation, mature fine oil sands tailings theoretical model

`

# DEDICATION

*Dedicated to*

*The Memory of My Grandmother*

`

# ACKNOWLEDGEMENTS

First of all, I would like to express my gratefulness to my supervisor, Dr. Julie Q, Shang for her help, trust, encouragement and outstanding instruction.

I would also like to show my appreciation to the faculty and staff in the Faculty of Engineering at the Western University, particularly to Ms. Stephanie Lawrence, Ms. Cynthia Quintus, Ms.Whitney Barrett, Ms.Caitlin Marshall, Ms. Melodie Richards and Mr. Erol Tas for their technical advice in the soil laboratory and help in the official work.

Further, I am very grateful for the friendship of my friends, Yu Guo, Raquibul Alam, Yifan Huang, Wenbing Wu, Steven Lin, Yuji Sano and Van Nuyen, who companied me through the difficult time, encouraged me during my research as well as made this period of time pleasant and enjoyable. Also, special gratitude is given to Conghan Sun, Changqing Gong and Xi Wang, who inspired me during my modelling work and gave me invaluable assistance.

Last but not least, I would like to show my great gratitude to my family for their understanding and support.

`

# TABLE OF CONTENTS

`

`

`

`

# LIST OF TABLES

`

`

# LIST OF FIGURES

## CHAPTER 2 BACKGROUND AND LITERATURE REVIEW



## CHAPTER 3 EK-VACUUM CELL TESTS ON MATURE FINE TAILINGS

`



**CHAPTER 4 THEORETICAL MODELING**

`

# LIST OF ABBREVIATIONS AND SYMBOLS

ASTM: American Society for Testing and Materials

DC: direct current

e: void ratio

$e_0$: initial void ratio

EK: electrokinetic

EO: electroosmosis

E: treatment with EK alone

V: treatment with vacuum pressure alone

S: treatment with surcharge preloading alone

ES: treatment with EK and surcharge loading

EV: treatment with EK and vacuum pressure

EMC：EK enhanced mechanical forces consolidation

I: electric current [A]

j: electric current density [$A/m^2$]

$k_e$: coefficient of electroosmotic permeability [$m^2$ /SV]

$k_h$: hydraulic conductivity [m/s]

`

n: porosity [-]

P: power consumption [kWh/$m^3$]

Q: electroosmotic flow rate [$m^3$/s]

U: voltage [V]

u: pore water pressure [kPa]

$\gamma_w$: unit weight of water [kN/$m^3$]

$\zeta$: zeta potential [mV]

$p_v$: vacuum pressure [kPa]

$s_u$: undrained shear strength [kPa]

MFT-A: mature fine tailings from another site in northern Alberta

MFT-B: mature fine tailings from northern Alberta

`

# Chapter 1 INTRODUCTION

## 1.1 General

Fine grained portions of oil sands tailings, known as mature fine oil sands tailings (MFT), are the by-products of mining industry. When the solid content of fine tailings once reaches around 30%, the compression of MFT becomes very slow (Jeeravipoolvarn 2010). Because of the possible environmental impacts, management and treatment of the slurry-like tailings are the major challenges faced by the mining industry.

The effect of electrokinetic dewatering (EK) on MFT has been studied by Guo and Shang (2014). Moreover, the vacuum treatment on clay has been studied for geotechnical engineering applications (Shang 1998 and Liu et al 2014). Though the combined EK and vacuum pressure treatment has been applied in the field test for the strengthening of soft clay (Mahfouz 2013), the analysis of its effect on the dewatering of MFT has not been conducted. In this research, an EK-vacuum cell was developed. A series of tests in this newly designed cell was introduced and the effect of the combined method on MFT was discussed. Furthermore, based on the small strain theory, the one dimensional consolidation model including the action of surcharge loading, vacuum pressure and electroosmotic consolidation was derived and the result of the model was compared with that from tests for verification and validation.

`

## 1.2 Objective of Study

The aim of this research is to: 1) evaluate the feasibility of EK combined vacuum pressure dewatering on MFT; 2) evaluate the dewatering efficiency of the combined application of the vacuum pressure and EK treatment; 3) carry out the analytical modelling to simulate the consolidation process under the combined effects of surcharge, vacuum pressure and EK treatment; and 4) assess the applicability of the analytical model by comparing the results with those from experiments.

During the experimental period, a series of index property tests was performed for the material characterization. EK cell tests were conducted to measure the coefficient of electroosmosis permeability (EO permeability) of MFT. The parameters obtained from these tests were used to verify the feasibility of this dewatering approach and promote the development of the analytical model. After the parameter study, a series of dewatering tests was conducted in the EK-vacuum cell. The results were used to assess the feasibility and efficiency of the combined method.

Finally, an analytical model based on the boundary conditions of the EK–vacuum cell was established. The consolidation behavior observed from the model based on the small strain theory was compared with that from experiments to verify the validity of the model.

## 1.3 Outline of Study

The thesis contains six chapters.

`

Chapter 2 reviews the background of MFT. It includes the mining process, the common properties of MFT and the general dewatering methods for MFT. The details about the principle, modelling and application of vacuum pressure and EK treatment on dewatering of soils are described.

Chapter 3 presents the experiments for evaluating the feasibility and efficiency of the combined EK and vacuum treatment on MFT. The characterization tests including physical and chemical properties are performed. The EK cell test for the coefficient of EO permeability to assess the feasibility of EK treatment on MFT is undertaken. The experimental apparatus and procedure of the EK-vacuum cell tests developed for the dewatering of MFT-B under combined effect of EK and vacuum pressure are also described. The effects of the combined actions of EK and vacuum on the water flow, settlement, undrained shear strength, water content, Atterberg limits and power consumption are discussed.

Chapter 4 presents one dimensional consolidation analytical model for evaluating the effect of surcharge loading, vacuum pressure and EK treatment on the consolidation of MFT. An equation in terms of the applied surcharge loading, vacuum pressure and EK is derived to estimate the consolidation behavior of MFT under the combined method. Furthermore, a comparison between the theoretical model and the results from the test has been made to verify the validity of the model.

Chapter 5 presents the summary of the thesis, the conclusion of the research and the recommendations for the future study.

`

## 1.4 Original Contributions

The original contributions of this study are shown as follows:

- The study of the feasibility and efficiency of EK combined vacuum pressure dewatering on MFT in a newly developed EK-vacuum cell.
- The derivation of an analytical one dimensional model to estimate the consolidation behavior of MFT due to the combined effect of electroosmosis, surcharge loading and vacuum pressure. This model is based on the boundary condition in which the drainage of these three methods is in the same downward direction.
- The applicability of this model in estimating consolidation behavior of MFT under the combined method is verified and comments are made on its feasibility.

`

# CHAPTER 2 LITERATURE REVIEW

## 2.1 Introduction and Objective

This chapter starts with a brief review of the background of the oil sands mining history. It includes the technology applied in the bitumen extraction, the origin of mature fine oil sands tailings (MFT) and the disposal approaches for MFT. The technologies for the dewatering of mature fine tailings are introduced. The consolidation techniques of geo-materials by vacuum pressure and electroosmosis are also reviewed. It includes the principles and applications of vacuum pressure. The principle, EK phenomena, essential parameters and applications of EK treatment are also interpreted for the better understanding of electrokinetics.

## 2.2 Oil Sands Mining Operations and Origin of Mature Fine Tailings

Oil sands, discovered in Northern Alberta, Canada in 1760s, are processed to recover crude oil and other petroleum products (Jeeravipoolvarn 2010 and Hande 2014). The oil sand deposits consist of sand, clay, water, and high molar mass viscous bitumen (Cabrera 2008). One of the commercial methods for oil sands mining is hot-water extraction process, which was initiated by Dr. Clark in 1929. During this process, bitumen is separated from oil sands under the combined effect of hot water, steam and sodium hydroxide (NaOH) (Jeeravipoolvarn 2010). The tailings stream is pumped to the large tailings ponds after extraction, in which three zones are developed (Cabrera 2008). Fig 2.1 shows the scenario of this process and Fig 2.2

`

shows the distribution of the three zones. The top zone is the clear supernatant water that can be recycled. Beneath this layer the second zone of immature fine tailings mixed with settling particles and water forms. The third zone is the MFT deposit on the bottom of the tailings pond. This zone is of the thickest layer among the three zones and it takes decades for MFT to reach the consistency of solids (Cabrera 2008 and Jeeravipoolvarn 2010).

## 2.3 Mature Fine Oil Sands Tailings

In Alberta, oil sands mainly deposit in three areas, i.e. Athabasca, Cold Lake and Peace River (Jeeravipoolvarn 2010). Fig 2.3 shows the distribution of oil sands area in Alberta. 64% of the oil sands areas (90,000 $km^2$ out of total 140,000 $km^2$ oil sands deposit) are managed to produce crude bitumen according to the data recorded (Alberta Energy 2015). It is recorded that 2 barrels of MFT can be produced for every barrel bitumen (i.e. 0.32 $m^3$ of MFT is generated for every barrel (0.16 $m^3$) of bitumen produced) (Hande 2014).The large quantities of tailings, therefore, are produced during the extraction of crude bitumen and the volume of the tailings produced is larger than that of oil sand mined (Cabrera 2008). It was reported at the end of 2013 that the tailings ponds covered 220 square kilometers, which was much larger than the anticipated 176 square kilometers (BGC 2010 and Alberta Energy 2014). It is estimated that two billion cubic meters of tailings will be generated by 2034 (BGC 2010). In addition to the large quantities, environmental issues are raised in disposal and management of MFT. Toxicity is one of the environmental issues (Brown 2013).

`

For example, naphthenic acids in the tailings pond are from bitumen extraction process. This acute toxicity is resistant to degradation and can keep toxic at low concentrations such as 16m/L (McMartin 2003 and Allen 2008).These chemicals may infiltrate into the surface or seep into the surrounding soils. The local ecology and groundwater condition then will be affected in a long term (MacKinnon and Boerger 1986 and Brown 2013).

Slow consolidation is another problem generated by MFT. Though the maximum solid content observed in the tailings pond can reach as high as 85% (Brown et.al 2013), it takes years to decades for MFT to consolidate to that extent due to the low permeability. MFT, therefore, often has low solid content and extremely low strength.

To sum up, the challenges faced by the oil sand industry include:

- Dewatering of MFT
- Improving the quality of recycled water
- Accelerating reclamation of MFT disposal areas

Legislation and policies related to the management of oil sands tailings are outlined in the Alberta Public Agencies Governance Act, Conservation and Reclamation Regulation and Environmental Protection and Enhancement Act etc. Within these polices, a series of guidelines has been proposed on reclamation, monitoring and reporting of tailings treatment (Alberta Energy Regulator 2015). Based on these guidelines and directives, various approaches have been suggested to

`

meet the requirement. These methods will be introduced in the following sections.

## 2.4 Property of Mature Fine Tailings

The major clay minerals in the MFT are kaolinite and illite (Owolagba 2013). Because of the water based extraction process, the tailings are the mixtures of sand, silt and fine clay particles suspended in water (Guo and Shang 2014). High water content, which is up to 180%, can be observed in MFT (Guo and Shang 2014). On the other hand, the average solid content of MFT is around 33% in tailings ponds, equivalent to an average void ratio of 5 (BGC 2010). In addition, MFT contains 3% (±2) uncovered residual bitumen by weight suspended in water (Owolagba 2013).

The MFT deposit in tailings ponds has very low shear strength, which is typically much less than 1 kPa (BGC 2010). The hydraulic conductivity of the MFT is in the range of $10^{-6}$ to $10^{-9}$ m/s, which indicates the extremely slow consolidation (BGC 2010). MFT is the geo-material with moderate plasticity. The liquid limit of MFT ranges from 40% to 75% while plastic limit is from 10% to 20% (Guo and Shang 2014).

# 2.5 Tailings Dewatering Technologies

## 2.5.1 Dewatering of oil sands tailings

Dewatering of oil sands tailings is one of the challenges faced by the industry. As is recorded, one barrel of bitumen production needs about 12 barrels of water. 30% of these barrels of water remain in the tailings and are tied up in the pore spaces

`

(Cabrera 2008). Dewatering of oil sands tailings, therefore, is the priority in tailings management.

In the soil and water system, water can be divided into the following sections (Smollen and Kafaar 1994).

- Free water: water not associated with solid particles;
- Interstitial, capillary: mechanically bound water which is trapped in the flocs;
- Vicinal: physically bound multiple layers of water molecules, held tightly to a particle surface by hydrogen bonding.
- Chemically bound or water of hydration.

Conventional technologies based on mechanical pressure can remove free water. Vicinal water, capillary water and free water can be discharged by the electroosmosis dewatering (Mok 2006). Considerations include factors such as dewatering efficiency, cost and time consumption should be made for the selection of an appropriate method to treat MFT. Fig 2.4 shows the different types of water removed in the different stages of dewatering.

### 2.5.2 Technologies Summary and Description

Numerous dewatering processes for the treatment of MFT have been investigated at various stages including the conceptual, research, pilot scale and commercial scale levels (Owolagba 2013). The common standards for the selection of technologies are as follows (Hande 2014),

`

- The solid content and shear strength required by the government should be met.
- The risks and hazards associated in the technology should be minimized.
- The technology must be cost effective and time efficient.

The most frequently applied technologies are summarized in Table 2.1. They can be mainly divided into five categories (BGC 2010 and Islam 2014), i.e.:

- Natural Process
- Mixtures/Co-disposal
- Physical/Mechanical
- Permanent Storage
- Chemical Treatment

Technologies in these classifications are discussed and analyzed from the fundamental and practical points of view in the following section.

**Permanent Storage**

Pit Lake or End Pit Lake is one type of the permanent storages. MFT can be pumped into the mined out pits and covered with water to form the Pit Lake (Hande 2014). The Pit Lake, in a long run, finally becomes a self-sustaining and functional ecosystem (BGC 2010). This process, however, takes long time and the water in the pit can be carcinogenic and threaten wild life (Hande 2014).

**Natural Process**

Sedimentation or self-weight consolidation relies on gravity to separate solids

`

from water (BGC 2010, Hande 2014 and Islam 2014). This technology requires large area and the process is slow (BGC 2010 and Hande 2014). The freeze-thaw technology consists of freezing the multiple thin tailings slabs in the winter and thawing in the following summer (BGC 2010 and Islam 2014). It has been recorded that under the effect of freeze-thaw cycles, a considerable amount of water can be released from MFT with layers of 5cm to 15cm thick (Dawson et al 1999).

**Physical/Mechanical Process**

The centrifuge technology is adapted for tailings dewatering (BGC 2010). The fluid is extracted from a material with the application of acceleration up to several times of gravity (Owolagba 2013). The final solid content of tailings can increase to about 60% (Islam 2014). The future work is needed to reduce the high upfront capital, operating costs and power consumptions (BGC 2010 and Islam 2014).

Vacuum preloading is the technology for the consolidation of highly compressive soft clay soils (Mohamedelhassan 2002). The vacuum pressure in the geo-materials generates a negative pore water pressure, which leads to the expedited consolidation (Mohamedelhassan 2002 and Torghabeh 2013). A detailed introduction of vacuum pressure consolidation is presented in section 2.6.

The electrical treatment technology is the application of a direct current (DC) to the clay slurry (BGC 2010). When the electric field forms, negatively charged clay particles will move to the anode and water will flow towards the cathode. It results in the dewatering and consolidation of soils. A systematic review of electrokinetics is

`

described in section 2.7.

**Chemical Treatment**

Coagulants (e.g. gypsum and lime) and flocculants (e.g. polymers) are widely used for the chemical treatment of oil sands tailings (BGC 2010, Brown 2013 and Islam 2014). Comparatively higher solid content of oil sands tailings can be obtained with the chemical additives injected (Jeeravipoolvarn 2010 and Islam 2014). In the meantime, the duration of sedimentation and consolidation can be reduced (BGC 2010). However, the chemical reagents generated may have adverse effects on water quality and the operational cost can be high.

**Mixtures/Co-disposal**

Composite and consolidated tailings (CT) are the promising methods developed in the University of Alberta (Islam 2014). Coarse sand is added to MFT in diverse sand to fines ratios (SFR) along with an amendment (typically gypsum) to form non-segregating slurry (BGC 2010, Hande 2014 and Islam 2014). After the treatment, a solid content that is as high as 60% can be obtained (Hande 2014). Since 1995 when Suncor firstly applied the CT process on a commercial basis, the commercial use of this method has continued for years (BGC 2010). But it is still under investigation for reducing energy consuming and being more environmentally friendly (Islam 2014).

`

## 2.6 Vacuum Pressure Dewatering

### 2.6.1 Introduction

The vacuum consolidation theory was first proposed by Kjellman in 1952 (Masse et al 2001) for the consolidation of clays and other ultra-soft soils (Rujikiatkamjorn et al 2007, Chu 2008 and Basack 2011). The principles, analytical model and applications of vacuum treatment are discussed in this section.

### 2.6.2 Principle

The conventional spring analogy is used to illustrate the consolidation process under vacuum pressure (Yan and Chu 2005 and Robinson et al 2012), as shown in Fig 2.5. The vacuum pressure leads to the increase in the effective stress and the dissipation of pore water pressure in the soil under a constant total stress. The final effective stress is equal to the applied vacuum pressure. It has been proved from the lab tests that the settlements caused by the vacuum pressure and by the surcharge loading of equal magnitude are identical (Mohamedelhassan 2002)

Further, the lateral movement generated by the vacuum pressure has been studied (Indraratna and Hudson 2005 and Robinson et al 2012). As is shown in Fig 2.6, the generation of tension zone is attributed to the inward movement close to the surface due to the suction (Robinson et al 2012). The suction can reduce the risk of shear failure (Indraratna and Hudson 2005).

`

### 2.6.3 Modelling

To validate the vacuum consolidation theory, one dimensional model has been developed (Mohamedelhassan 2002 and Chai and Carter 2013). The excess pore water pressure generated by the vacuum pressure is expressed as (Mohamedelhassan 2002),

$$u(z,t) = p_v\left\{1-\sum_{n=0}^{\infty}\left(\frac{4}{(2n+1)\pi}\sin\frac{(2n+1)\pi z}{2h}\right)\cdot\exp\left[-\left(\frac{2n+1}{2}\right)^2\pi^2\frac{c_{vc}t}{h^2}\right]\right\} \qquad [2.3]$$

Where $c_{vc}$ ($m^2/s$) is the coefficient of consolidation for vacuum preloading, z (m) is the depth, h(m) is the drainage path, $T_v$ (-) is the time factor and $p_v$ (kPa) is the constant vacuum pressure.

### 2.6.4 Applications

Successful field applications of vacuum preloading in the treatment of soft clays have been reported (Shang et al 1998 and Raison et al 2000). The cases of the ground improvement in Xingang Port (Shang et al 1998) and Yaoqiang Airport runway (Tang and Shang 2001) show that vacuum preloading is effective in treating very soft and highly compressive clayey soils. The results of the accelerated consolidation and four-fold increase in the undrained shear strength of soil soils were observed (Shang et al 1998). Other successful applications of the combined vacuum pressure and surcharge loading treatment on treating soft soil have been reported (Mohamedelhassan 2002 and Saowapakpiboon et al 2011). The consolidation process takes place quickly without the risk of shear failure because the positive excess pore

`

water pressure induced by the surcharge loading is balanced by the negative vacuum pressure (Griffin and O'Kelly 2014).

The field tests reported in the open literature include two approaches, i.e. preloading with membrane seal and without membrane. Typically, the clay slurry of the low permeability is placed as a sealing cap in a membrane-free system (Chu 2008, Karstunen 2008 and Parsa 2014), as shown in Fig 2.7. Yan and Cao (2005) have elaborated the application of slurry sealing cap in the vacuum preloading system, which is used in the offshore projects. However, the tension cracks may appear near the surface and affect the vacuum pressure distribution (Yan and Cao 2005).

## 2.7 Electrokenetics

### 2.7.1 Introduction

Electrokenetics (EK) was firstly observed by Reuss (1809). It can be observed that water moves from anode towards cathode when a direct current (DC) is applied in a clay-water system (Lee 2000 and Soga and Mitchell 2005). In this section, the basic concepts rooted in the EK are discussed. The EK dewatering and electrochemical effects are introduced. The analytical model of electroosmosis dewatering is reviewed and the applications of EK treatment are illustrated.

### 2.7.2 Electrokinetic Phenomena

Double layer theory is one of the fundamental theories in the EK system. The prerequisite for the existence of the double layer is the charged surface of soil

`

particles and isomorphic substitution is one of the major reasons to interpret the reason of soil surface charge.

Tetrahedral and octahedral sheets are the two major types of clay mineral units. In the tetrahedral unit, one silica atom is trahedrally coordinated with four oxygens and one magnesium or aluminum is coordinated with oxygens or hydroxyls in the octahedral unit. Because of the structural imperfection, cations such as silica, magnesium or aluminum in the center of these structures are substituted by those with lower valence. Clay particles, therefore, are negatively charged (Soga and Mitchell 2005). The positively charged ions are absorbed to the particle surface to balance the negative charge on the soil particles surface. These two layers form the basic concept of the double layer theory (Sparks 1998).

Many double layer models have been developed to reasonably illustrate this theory. Among them, Helmholtz model, Gouy-Chapman model and Stern model are the widely accepted ones.

**Helmholtz Model**

Helmholtz model is one of the earliest models popularly used. It was firstly proposed by Helmholtz (1879). In this model, radii of the pores are assumed to be larger than the thickness of the diffuse layer. On the other hand, counter ions are concentrated near the surface. The distance between the surface and the countercharges are thought to be small. Therefore, it can be regarded as an electrical condenser near the surface of the wall (Soga and Mitchell 2005). Because of this

`

limitation, Helmholtz model is not acceptable to consider the diffusion effect and the double layer is thought to be fixed (Soga and Mitchell 2005).

**Gouy-Chapman Model**

In 1910 and 1913, Gouy and Chapman discovered the diffusion tendency of the high concentrated cations near the surface of soil particles to reach the equilibrium of the system. Diffusion factor is taken into account in this model. The ions in the model, however, are assumed to be point charges and allowed to move towards to the surface limitlessly. This results in an absurdly high concentration of ions near the surface (Sparks 1998 and Mok 2006).

**Stern Model**

To improve Gouy and Chapman model, finite size of ions is considered in the Stern model (Lee 2000). The double layer region is divided into two parts—inner area is a fixed layer where ions are adsorbed and outer layer is a diffuse layer. The interface of these two layers is the shear plane called Stern layer (Lee 2000).

Based on the double layer theory and considering the coupling effects of the electrical and hydraulic flow, four electrokinetic phenomena can be expressed (Soga and Mitchel 2005). They are electroosmosis, streaming potential, electrophoresis and migration potential. Fig 2.8 shows schematics of these phenomena and Table 2.2 lists detailed information. Under the effect of electric field, electroosmosis and electrophoresis happen. Electroosmosis is the water movement in a porous medium under the direct current. When an electrical field is applied, free ions in the pore water

`

migrate to the electrodes of opposite charge while dragging hydrated water molecules around them. Electrophoresis is the movement of the solid under the effect of electric field. The negatively charged particles move towards the anode when the direct current is applied. On the other hand, streaming potential and migration potential take place under the effect of hydraulic force or gravity force. Streaming potential is the electrical potential difference generated when the water moves through the soils under the hydraulic gradient and migration potential is the potential difference generated when the charged particles settle under the action of gravity (Lee 2000 and Soga and Mitchell 2005).

### 2.7.3 Electrochemical Effects

When an electric current is applied to the water-electrolyte system, electrolysis reactions take place in both electrodes (Lockhart 1983, Lee 2000 and Soga and Mitchell 2005). In the anode, electrons are given up and oxygen gas is generated,

$$2H_2O - 4e^- \rightarrow O_2 \uparrow + 4H^+ \qquad [2.4]$$

In the cathode, electrons are received and hydrogen gas is generated,

$$4H_2O + 4e^- \rightarrow 2H_2 \uparrow + 4OH^- \qquad [2.5]$$

The generation of $H^+$ in the anode reduces pH value and the evolution of $OH^-$ in the cathode increases pH value (Soga and Mitchel 2005 and Mok 2006). The acidic zone in the system expands because protons driven by the electrical current in the anode move towards the cathode (Mok 2006 and Elazar 2011).

`

### 2.7.4 Electroosmosis Dewatering Process

Electroosmosis dewatering process includes more than one EK phenomenon. Among them, electroosmosis and electrophoretic effects are the major ones. This process mainly contains three steps and it was described in some researches (Mok 2006). Firstly, particles can move freely in the fluid suspension system. Electrophoretic effect is phenomena during this stage. Once the particles are locked in position and cease moving, the electrophoretic effect will reduce and the electroosmosis effect comes to take charge of the dewatering process. During this period, electrochemical effect can be observed around the electrodes as mentioned above. Finally, electroosmosis dewatering process will end because liquid phase in the system is not continuous as the result of dewatering (Mok 2006).

### 2.7.5 Essential Parameters and Basic Analytical Model

Some basic parameters are needed to quantitatively interpret electroosmosis phenomenon. They include the zeta potential, the quantity of liquid discharged by electroosmosis, the coefficient of electroosmosis permeability and the electrical potential gradient etc. Besides, analytical consolidation model has been established by many researchers to estimate the consolidation behavior for electroosmosis. They will be shown in the following section.

**Zeta Potential**

According to the Hemholtz-Smoluchowski model, zeta potential ($\zeta$) is one of

`

the factors determining the electroosmotic flow (Asadi et al 2013). It is supposed to be the electric potential at the solid-liquid interface when particles move. In the double layer model, it is assumed to be the potential between the fixed and mobile layer, i.e. the shear plane between the Stern layer and Gouy layer in the Stern-Gouy model as shown in Fig 2.9. It is assumed that diffuse layer will be moveable. The location of the shear plane, therefore, is unknown (Shang et al 1994).

In the Helmholtz-Smoluchowski model, zeta potential is expressed based on the hypothesis that it is proportional to the electroosmosis flowing rate. This relationship can be expressed as below (Soga and Mitchell 2005),

$$\zeta = \frac{4\pi\eta}{DE} v_e \qquad [2.6]$$

Where $\eta$ ($Ns/m^2$) is the viscosity, D(F/m) is the relative permittivity, E(V/m) is the surface potential and $v_e$ (m/s) is the flow velocity induced by electricity.

It is clearly that the ion exchange capacity, the ion radius size and the thickness of double layer have influence on the magnitude of zeta potential.

**Quantity of Electroosmosis Flow**

Casagrande (1952) has processed the expression among the quantity of liquid, the coefficient of electroosmosis permeability and the electrical potential gradient based on the previous field experience and foundation application. It can be analogous to Darcy's hydraulic flow equation and described as below,

$$Q_e = k_e i_e A \qquad [2.7]$$

`

where $Q_e$ ($m^3/s$) is the electroosmosis flow rate, $k_e$ ($m^2/sV$) is the coefficient of electroosmosis permeability which can only be determined by the experiment in reality, A ($m^2$) is the section area and $i_e$ (V/m) is the electrical potential gradient that could be illustrated as,

$$i_e = \frac{\Delta E}{\Delta L} \qquad [2.8]$$

Where $\Delta$ E(V) is the difference of electric field intensity and $\Delta$ L (m) is the difference in distance.

**Coefficient of Electroosmosis Permeability**

In the theoretical model expressed by Helmholtz and Smoluchowski, the value of the coefficient of electroosmosis permeability, $k_e$, can be hypothetically illustrated as following (Soga and Mitchell 2005),

$$k_e = -\frac{\varsigma D}{\eta} n \qquad [2.9]$$

Where $\zeta$ (V) is the zeta potential, n is porosity, D(F/m) is the relative permittivity and $\eta$ ($Ns/m^2$) is the viscosity.

The relative permittivity and viscosity are assumed to be constants. Porosity and zeta potential, therefore, have influence on the coefficient of electroosmosis permeability.

**Consolidation Model**

The analytical model of electroosmosis consolidation is based on several

`

assumptions, i.e. the soil is saturated, chemical properties of the soil remain unchanged and electrophoresis is negligible, which means the movement of solids is not considered.

The original governing equation was derived by Casagrande (1952). Esrig (1968) derived the solution of pore water pressure based on the boundary condition of closed anode and opened cathode,

$$u = \frac{k_e}{k_h}\gamma_w U(x) + \frac{2k_e\gamma_w U_m}{k_h\pi^2}\cdot\sum_{n=0}^{\infty}\frac{(-1)^n}{(n+1/2)^2}\sin[\frac{(n+1/2)\pi x}{L}]\cdot\exp[-(n+\frac{1}{2})^2\pi^2 T_v] \quad [2.10]$$

Where u (kPa) is the excess pore water pressure, $k_e$ ($m^2$/sV) is the coefficient of electroosmosis permeability, $k_h$ (m/s) is the hydraulic permeability, $U_m$ (V) is the maximum voltage, U(x) (V) is the voltage at distance x, $\gamma_w$ (9.8kN/$m^3$) is the unit weight of water, L (m) is the distance between anode and cathode and $T_v$ (-) is the time factor.

**Electroosmosis Permeability Ratio**

The electroosmosis permeability ratio, $k_e/k_h$, governs the effectiveness of the electroosmosis consolidation (Mohamedelhassan 2002) because it determines the magnitude of the negative pore water pressure generated during the electroosmosis consolidation. The electroosmosis permeability ratio of the value that is larger than 0.1 is desirable in the EK treatment (Elazar 2011).

`

### 2.7.6 Effective Parameters

Parameters governing the effectiveness of electroosmosis include the electroosmosis ratio, the coefficient of electroosmosis permeability, the hydraulic conductivity and the power consumption. The parameters should be assessed for the feasibility of EK treatment on the soils. Typical ranges of these parameters for the fine-grained soil such as clays and silts suitable for EK treatment are summarized in Table 2.3 (Rowe 2001 and Mohamedelhassan 2002).

### 2.7.7 Applications

The applications of EK treatment, including soil remediation, consolidation and dewatering, are mainly for the soils with low permeability (Soga and Mitchell 2005 and Mok 2006). Electroosmosis dewatering has been reported by many researchers (Lo et al 1991, Micic et al 2001 and Elazar 2011). Also, the research on the EK dewatering on MFT has been conducted (Guo and Shang 2014).

The selection of electrode materials is based on several standards including minimum voltage loss, resisting corrosion and maximizing water transport. A detailed comparison has been made by Mohamedelhassan (2002) among different electrode materials such as iron, copper and carbon. It was reported that the metallic materials had lower voltage loss. In the traditional configurations, electrodes were allocated in a fixed position (Casagrande 1952, Esrig 1968 and Shang and Lo 1997). The influence of the provisionally reversed polarity was studied and the reversed polarity in the

`

midway of treatment period led to a more uniform result (Lo et al 1991and Bourgès et al 2014).

The concept of an electroosmosis cell system is adopted by some researchers (Asadi et al 2013). The apparatus often includes an electroosmosis cell, a loading plate to apply surcharge load, the anode and cathode reservoir as well as a volume measurement tube to collect the water discharged (Gopalakrishnan et al 1996, Shang and Lo 1997, Micic et al 2001 and Bourgès et al 2014).

Electroosmosis dewatering can be in conjunction with other mechanical methods such as surcharge preloading via vertical drains to enhance the effect of dewatering as well as to improve the mechanical properties of soil (Lo et al 1991). An analytical model was established for the combined effect of the surcharge loading and electroosmosis (Shang 1998). Moreover, a field trail adopting the electroosmosis consolidation and vertical drains was carried out by Chew et al (2004), during which electrically conductive vertical drains were applied. Furthermore, the combination of EK and vacuum pressure has been adopted in the lab tests and field trials to strengthen soft soils and improve the ground (Mahfouz 2013 and Liu et al 2014). The results reveal that with the aid of vacuum pressure, gases generated around electrodes can be pumped out easily and the electrical resistance will be reduced. Therefore, the dewatering efficiency is raised (Mahfouz 2013).

`

## 2.8 Summary

In this chapter, a general review of the technologies for MFT dewatering was presented, with focus on the principle and applications of vacuum preloading and EK treatment. It provided a promising basis for the effect of combined EK and vacuum pressure treatment on MFT.

`

Table 2.1 Major Tailings Dewatering Technologies in the Oil Sands Industry

| Type | Technology | Reference |
|---|---|---|
| Natural Process | Freeze Thaw | Johnson et al 1993 |
| | Evapotranspiration | Johnson et al 1993 |
| | Self-weight Consolidation | Priscu 1999 |
| Physical/Mechanical Process | Electrical Treatment | Guo and Shang 2014 |
| | Centrifuge | Owolagba 2013 |
| | Vacuum Pressure | Masse et al 2001 |
| Chemical/Biological Amendment | Thickening Process | Jeeravipoolvarn 2010 |
| | Chemical Treatment | Onyelowe and Okoafor 2012 |
| Mixtures/Co-disposal | Mixing Thickened Tailings with Sand | Jeeravipoolvarn 2010 |
| Permanent Storage | Pit Lakes | BGC 2010 |

`

Table 2.2 Procedure of Electrokenetics (Sennett and Olivier 1965)

| Procedure | Property Measured | Mobile Phase |
|---|---|---|
| Electrophoresis | Particle Mobility | Particle |
| Sedimentation Potential | Potential | Liquid |
| Streaming Potential | | |
| Electroosmosis | Pressure | None |
| | Velocity | Liquid |

Table 2.3 EK Treatment Parameters (Rowe 2001 and Mohamedelhassan 2002)

| **Parameter** | **Unit** | **Value** |
|---|---|---|
| **$k_h$, hydraulic conductivity** | m/s | $10^{-10} \sim 10^{-8}$ |
| **$k_e$, EO permeability** | m2/sV | $\sim 10^{-9}$ |
| **$k_e/k_h$ ratios** | m/V | $\geq 0.1$ |
| **p, hourly power consumption** | kWh/$m^3$h | 0.01-1 |

`

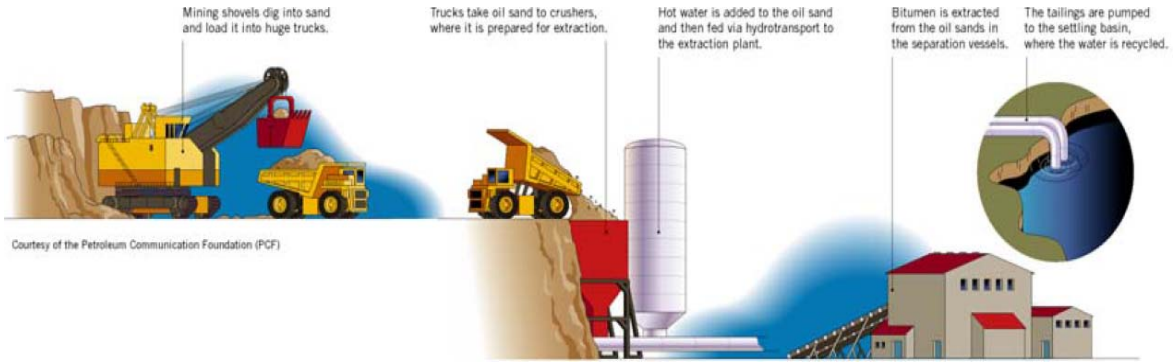


Fig 2.1 Simplified Mining Operations (Dunbar and Eng 2007).

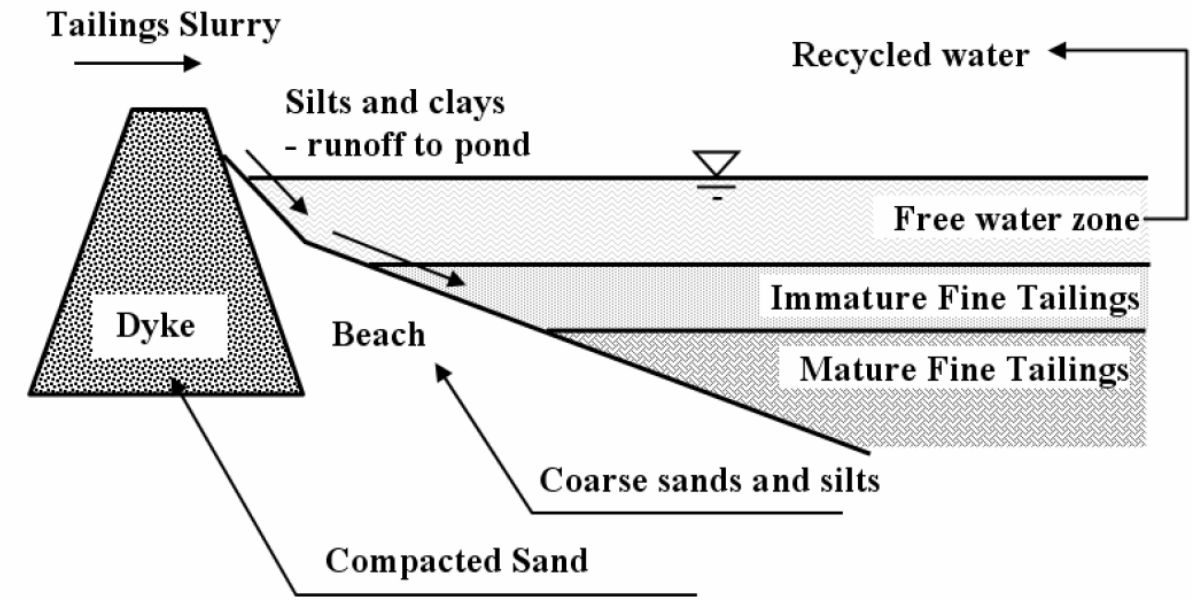


Fig 2.2 Cross Section of an Oil Sands Tailings Settling basin (Jeeravipoolvarn 2010).

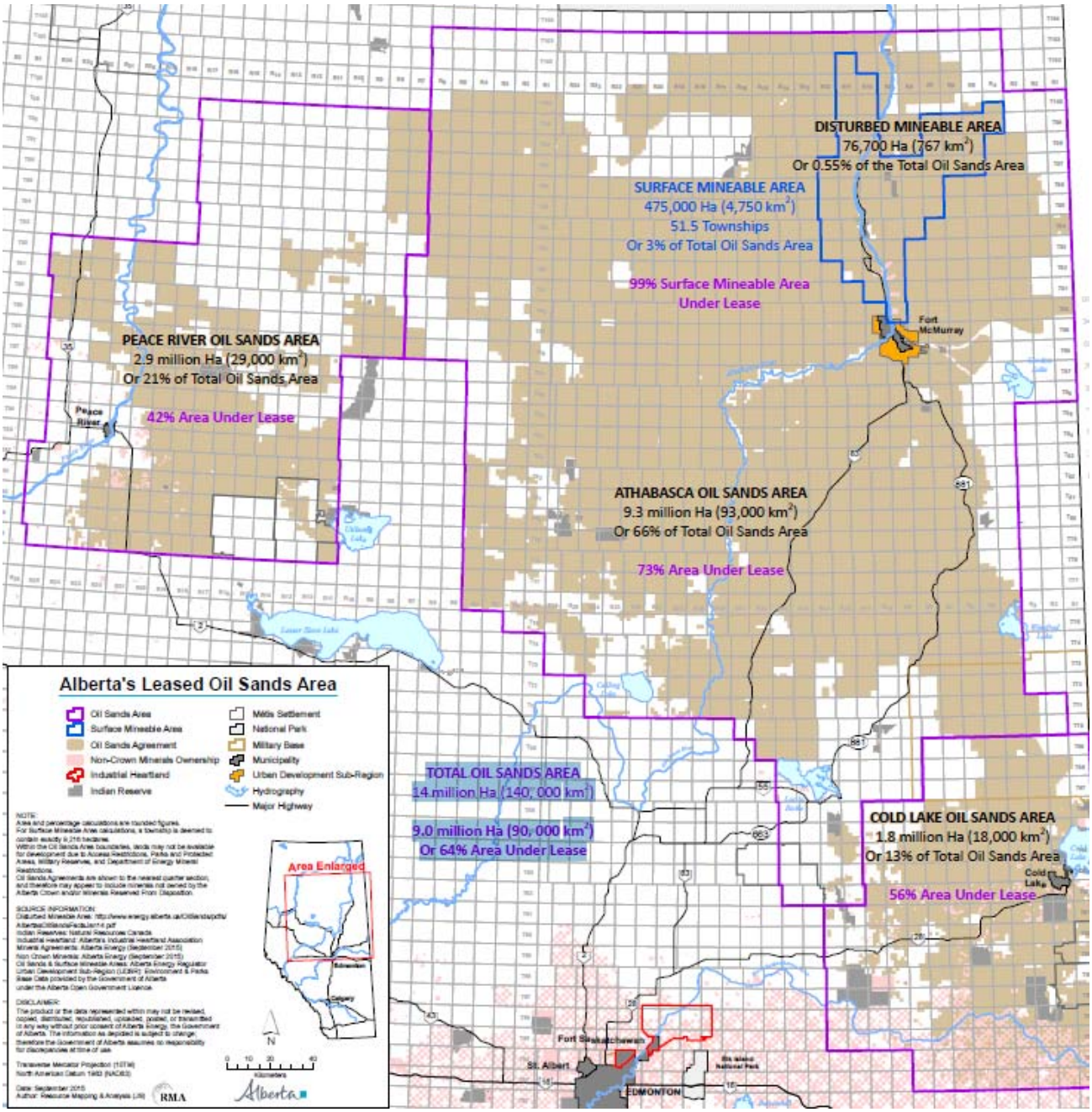


Fig 2.3 Distribution of Oil Sands Industry (Alberta Energy 2015)

`

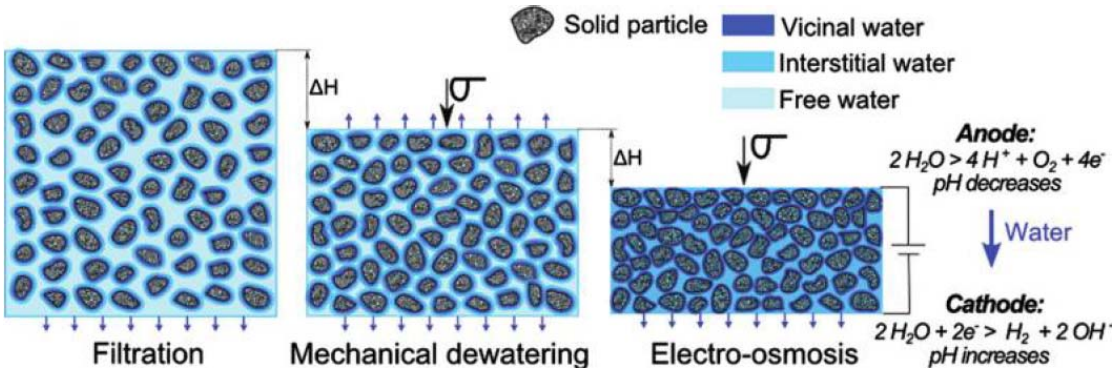


Fig 2.4 Schematic Representation of Different Stages of Dewatering (Bourgès et al 2014)

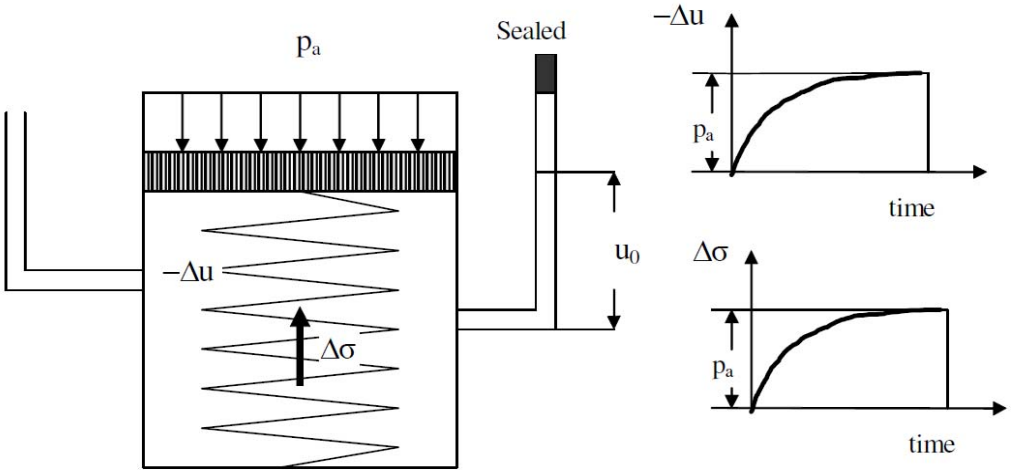


$$u_0 = p_a$$

$$\Delta\sigma = p_a - (u_0 - \Delta u) = \Delta u$$

Fig 2.5 Spring and Piston Analogy of Consolidation Response to Vacuum Pressure (Yan and Chu 2005)

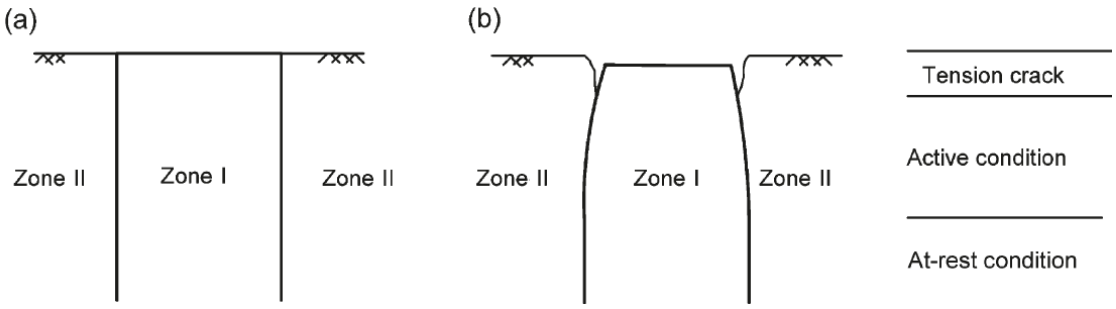


Fig 2.6 Ground condition (a) before and (b) after vacuum consolidation. (Robinson et al 2012)

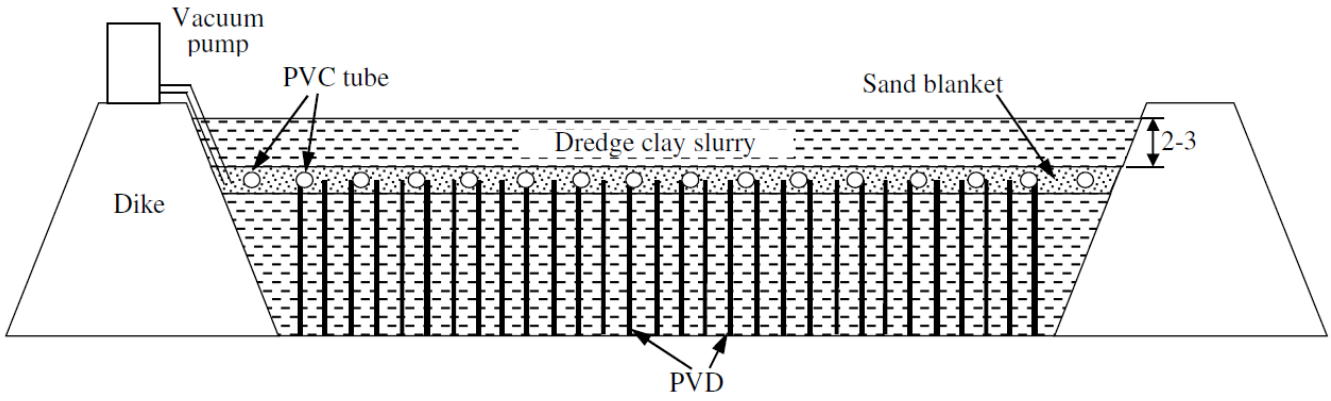


Fig 2.7 No Membrane Vacuum Preloading Method (Chu 2008)

`

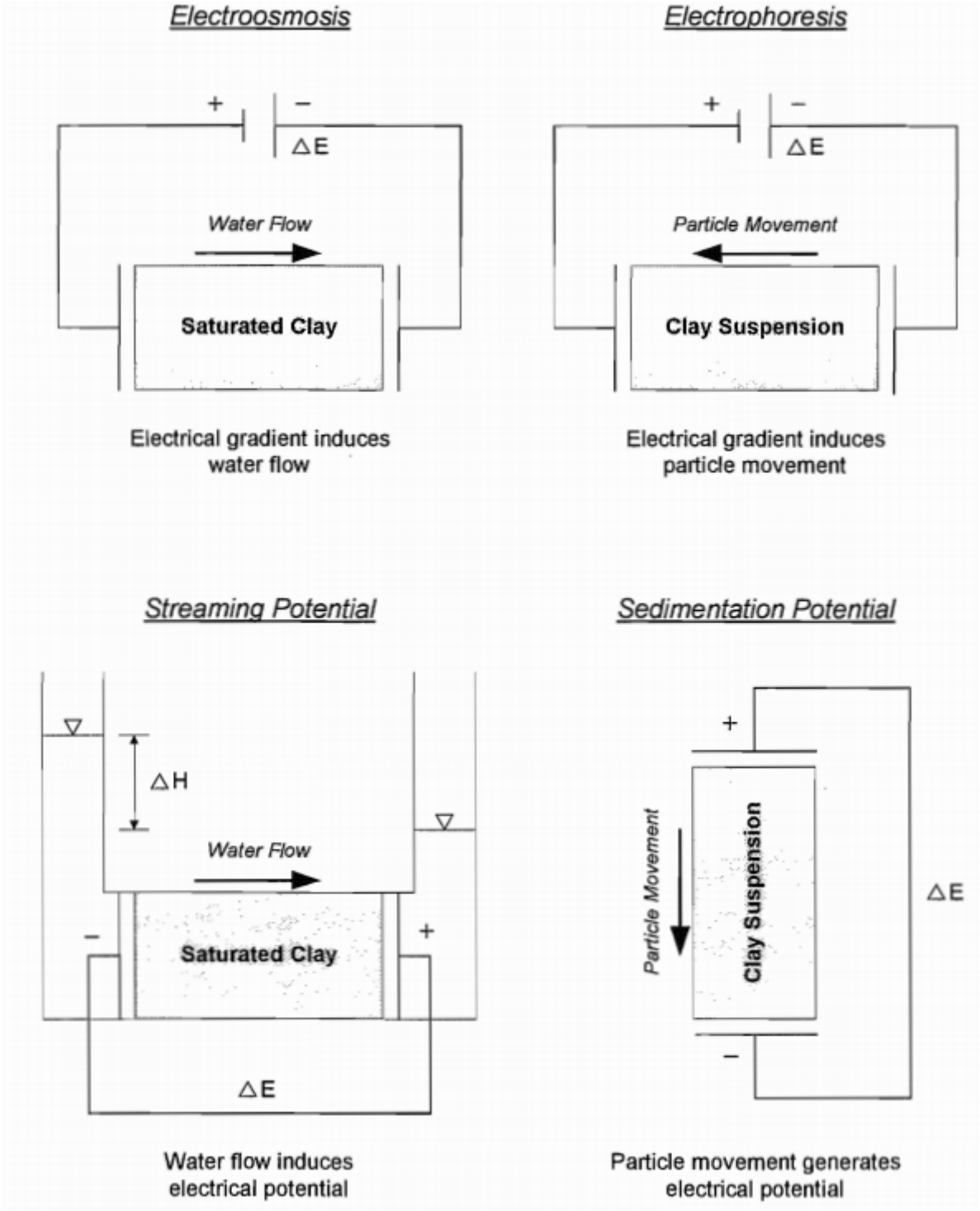


Fig 2.8 Electrokenetics Phenomena in Soils (Soga and Mitchell 2005)

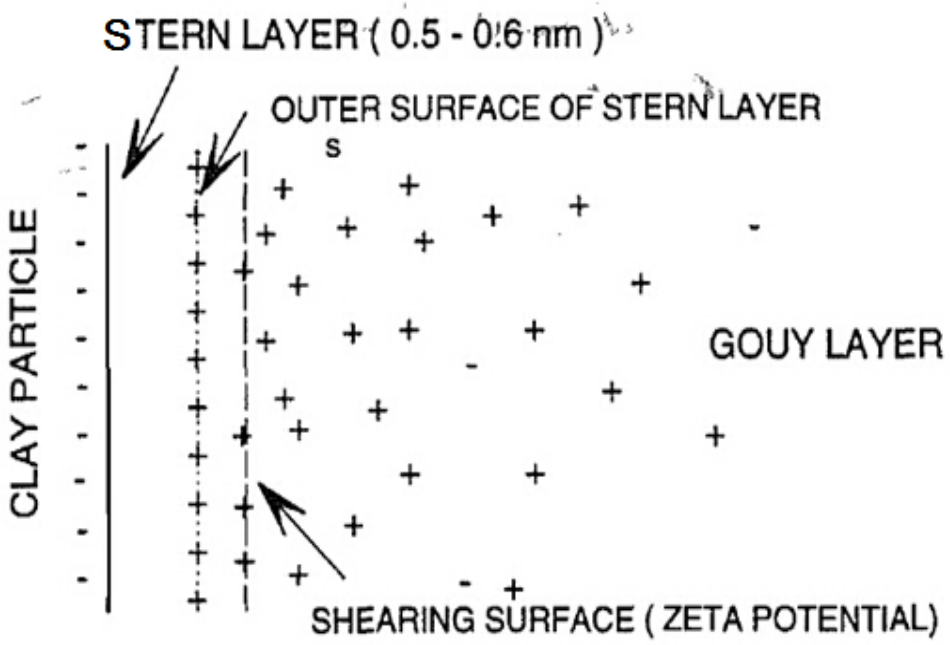


Fig 2.9 Stern-Gouy Double Layer (Shang et al1994)

`

# CHAPTER 3 EXPERIMENTAL STUDY

## 3.1Introduction

Mature fine oil sands tailings (MFT) are the by-products of oil sands mining. EK treatment has shown the potential in the treatment of MFT-A (mature fine tailings from northern Alberta). The mean water content after the treatment decreased from 171.3% to 63.9% (Guo and Shang 2014). In this chapter, mature fine tailings from another site in northern Alberta (MFT-B) are characterized and the properties of MFT-B are compared with those of MFT-A. A series of tests is carried out in a newly developed EK-vacuum cell. The cell is designed for one-dimensional settling and consolidation by combined action of EK, vacuum pressure and surcharge preloading. The effects of these actions are evaluated in terms of the water flow, settlement, shear strength, water content, power consumption and Atterberg limits.

## 3.2 Material Characterization

### 3.2.1 Introduction

In this section, the characterization of physical and chemical properties of MFT-B is presented and analyzed. The results are compared with those of MFT-A as well. Furthermore, the EK cell test for the measurement of the coefficient of electroosmosis permeability (EO permeability) is introduced.

`

### 3.2.2 Characterization Test

The characterization of MFT includes physical properties (water content, specific gravity, grain size analysis and Atterberg limits), mineralogical properties by X-ray diffraction test, and chemical properties (the zeta potential, pH value of MFT suspension, and water chemistry). The results are summarized in Table 3.1 and Table 3.2 and compared with those of MFT-B.

**Physical Properties**

MFT-B was provided in ten plastic pails, courtesy of Shell Canada Limited. MFT in these pails were than mixed in a large barrel. Samples have sticky and dark brown texture with a strong odor because of the existence of hydrocarbon. They are fluid-like with an average water content[1] of 188%±2%, which is higher than that of MFT-A (171.3%) (Guo and Shang 2014). The two tailings samples have similar specific gravity (2.51 of MFT-A and 2.49 of MFT-B). The liquid limit and plastic limit of MFT-B are 20.6 and 46.7, respectively. According to the unified soil classification system, MFT-B is classified as CL. MFT-B shares similar basic physical properties with MFT-A, as shown in Table 3.1. The result of grain size analysis is presented in Fig 3.1. It is noted that MFT-B contains 7% sand and the clay content (4%) is lower than that of MFT-A. On the other hand, MFT-B has higher silt content (89%) than that of MFT-A (80%).

[1]The water content, w(%), is defined as the mass of water in the soil to the mass of soil particles.

`

## Chemical Properties

### Carbonate Content and Organic Matter

The powdered MTF-B sample passing through #200 sieve had weak reaction with hydrochloric acid. The carbonate content of MFT-B, therefore, is less than 1% based on chittick test results (Dreimanis 1962).This result is same with that of MFT-A.

The organic matter is primarily attributed to residual bitumen in MFT. The content of organic matter was measured following ASTM D2974 (2015). The result shows that MFT-B has the organic matter content of 19.9% (mass ratio), which is higher than that of MFT-A (14.7%).

### Zeta Potential

Pulverized MFT samples passing #200 sieve were used for zeta potential measurement. One spoon of samples (around 0.1g) was well mixed with 30mL distilled water in a Model 75HT aquasonic. The suspension was then injected into an electrophoresis cell for zeta potential test in the zeta potential analyzer (Model ZetaPlus by Brookhaven Instruments Corporation) that has the capacity of measuring zeta potential from -150mV to 150mV. During the measurement, the pH value of the suspensions was adjusted from 2 to 12 by titration using 0.1M HCl and 0.1M NaOH. The relationship between zeta potential and pH value of suspension is plotted in Fig 3.2. It is shown that with the changes of suspension pH value, the zeta potentials of MFT-B vary from -20.3 mV to -37.3mV. The trend line of MFT-B is different from

`

MFT-A, whereas both have negative zeta potentials within a wide range of water pH values. The stable zeta potential in a broad pH range is an important indicator that the EK treatment on the material will be effective.

**Mineralogy**

The X-ray diffraction (XRD) test was conducted on MFT solids. MFT samples were stored into a tray and air-dried for 7 days at room temperature (22 $^{o}$C). These samples were then pulverized and passed a #200 sieve. The solids finer than 0.075mm were used for X-ray diffraction test, using a Rigaku diffractometer with a Co Kα radiation source (λ=1.79926 Å).

The result is shown in Fig 3.3.The minerals identified include illite, kaolinite and quartz. There is no difference in the mineralogy between MFT-A and MFT-B.

**Pore Water Chemistry**

The tailings pore water was squeezed and analyzed by ICP tests. The results are summarized in Table 3.2. MFT-A and MFT-B have similar concentrations of $Na^{+}$ and $Ca^{2+}$. However, concentrations of $Mg^{2+}$ and $K^{+}$ in the pore water of MFT-B are almost three times higher than those of MFT-A.

### 3.2.3 Electroosmotic Permeability

The EK cell test was carried out to measure the EO permeability of MFT-B under a preloading of 3kPa. The apparatus and testing procedure were based on the

`

one proposed by Guo and Shang (2014).The water flow, voltage drops and settlement were recorded to calculate the EO permeability. The schematic of the EK cell system is presented in Fig 3.4. The EO permeability of MFT-B is measured in the range of $2.77x10^{-9}$ to $4.95x10^{-9}$ $m^2/sV$, as shown in Table 3.3. It indicates that the EK treatment is effective on MFT-B.

## 3.3 EK-vacuum Dewatering Experimental Study

### 3.3.1 Experimental Apparatus

An EK-vacuum cell was designed and built for this study. The specifications of EK-vacuum cell and testing conditions are summarized in Table 3.4. The schematic and photo of the cell are presented in Fig.3.5 to Fig 3.7. The general configuration includes:

- An EK-vacuum cell made of 0.5 cm thick transparent Plexiglas tube is to host samples. The dimension (diameter×height) of the cell is 88 mm×190 mm;

- A water reservoir to collect water discharged is with the dimension (diameter× height) of 50 mm×150 mm;

- A vacuum control system of 60 kPa capacity consists of a vacuum line and a regulator. The vacuum line is connected to a vacuum gauge with a precision of 1kPa.

- The filter system is set up. It consists of a filter paper, two layers of geotextile and

`

a porous Plexiglas plate. A filter paper is placed at the bottom of the EK-vacuum cell. It is overlain by a layer of geotextile. A porous Plexiglas plate is placed on this geotextile and the other layer of geotextile is covered on the top of the plate. This system enables the free drainage and avoids the movement of solids.

The filter system was placed at the bottom of the EK-vacuum cell. The cathode made of a steel wire mesh (SS316) was placed on the top of the filter system. The sample was poured into the cell to the given height when the cathode was settled. A layer of geotextile was then put on the top of the sample and covered by the anode that was made of a steel wire mesh (SS316). Both anode and cathode were connected to the DC power supply. There were two ports in the water reservoir cell. One was on the top and the other was in the side wall. The port on the top was connected to the vacuum line directly and the other one in the side wall was connected to the bottom of the EK-vacuum cell for the application of vacuum pressure and water drainage, as shown in Fig 3.7.

### 3.3.2 Testing Procedure

Before each test, the water content of samples was measured. The initial water content was 188%±2%. Then the sample was poured into the cell to the height of 65mm between anode and cathode. In the tests with surcharge loading, the surcharge was applied gradually to avoid failure. In the tests with vacuum pressure, the test could start immediately. In each test, the current density, surcharge loading and vacuum pressure were maintained constant. Table 3.4 summarizes the conditions of all

`

the tests and Table 3.5 shows the detailed condition of each series.

The water discharged in the water reservoir and the vertical settlements were monitored in real time. They could be read directly from the scale on the cell. After the tests, the samples in the anode and cathode were carefully transferred out of the cell and collected for the measurement of water content and Atterberg limits. Because of the predominant dewatering effect, the shear strength of samples in the E3V series (E3V1, E3V2 and E3V3) with 15 $A/m^2$ current density could be measured by the pocket penetrometer (Model 29-3729). The tip of the penetrometer was pushed into the soil sample collected after the test at right angles to the surface. The unconfined compressive strength of samples in this series could be read directly from the scale on the penetrometer when the groove on the tip was even with the surface of the soil. The undrained shear strength then could be calculated. The result of the undrained shear strength tested is shown in Table 3.7.

## 3.4 Result and Discussion

The result of EK–vacuum cell tests is discussed in this section. It includes water content, Atterberg limits, undrained shear strength and power consumption. The settlement, water flow, current changes and voltage variation during the tests are also investigated.

### 3.4.1 Current and Voltage

Figs 3.8 (a) and (b) show the changes of voltage and current in real time during

`

the treatment in the E3 series (EK treatment with 15A/$m^2$ current density) and E3V series (EK and vacuum pressure combined treatment with 15A/$m^2$ current density). The current density was kept constant in the beginning in each test and the threshold voltage was set to be 30V.

As is shown in Fig 3.8, two stages can be observed. These stages are divided by $t_I$ and $t_v$. $t_I$ is about 5 hours and $t_v$ is the ending time of the tests, which can reach 48 hours. Between 0 and $t_I$, the current density controlled the tests. In this stage, the electric current was kept constant (0.09A). Corresponding to 15A/$m^2$ current density combined with 30kPa to 50kPa vacuum pressure, the voltage fluctuated slightly from 13V to 17V. Due to the generation of gases and the development of unsaturated zone, the electrical resistance of the MFT increased. Because of the Ohm's law, the voltage started to increase after 3 to 4 hours to the threshold 30V, and afterwards the treatment was under the constant voltage. Between $t_I$ and $t_v$, the test was under the constant voltage of 30V. The current decreased from the maximum value of 0.09A to near 0 with the continuous increase in the resistance, as shown in Fig 3.8.

### 3.4.2 Settlement and Flow

Figs 3.9 (a) and (b) present the changes of the normalized settlement and normalized water discharged in real time during the E3 test series, the V3 test series, the E3V1 test series, the E3V2 test series and the E3V3 test series. As is shown in Fig 3.9, the EK and vacuum combined treatment (EV series) has the most significant effect. The time consumed during the EV series was 30 hours in average, which was

`

much shorter than that of 48 hours in the treatment with the single method (E series or V series). On the other hand, the final settlement in the E3 series and V3 series was around 30% of the initial height of the sample. By contrast, the final settlement of approximately 50% to 60% of the initial height of the sample in the EV series with the combination of 15 $A/m^2$ current density and 30kPa to 50kPa vacuum pressure was twice larger than that in the E3 series and V3 series. With the aid of vacuum pressure, the volume of the water discharged in the EV series could reach 60% to 70% of the total volume of the sample. It was much larger than that in the E3 series (30%) and the V3 series (40%).

### 3.4.3 Water Content

The average initial water content of the MFT samples was 188%, with the maximum 190% and minimum 186%. The effects of the current density and vacuum pressure on the water content are shown in Fig 3.10 (a) and (b), respectively. As is shown in Fig 3.10 (a), the water content of MFT decreased linearly with the increasing current density under the constant pressure applied. The slope of the fitting line was -3% ($\Delta w\%/A/m^2$).Similar relationship between the vacuum pressure and water content can be observed in Fig 3.10 (b). Under the constant current density, the increase in the vacuum pressure led to the linear decrease in the water content. The slope of the fitting line is -0.9% ($\Delta w\%/kPa$).

The effects of the treatment method on the water content after the tests are presented in Table 3.6 and Fig 3.11. As is shown, the EK and vacuum combined

`

treatment (EV series) is the most effective. The final water content of the sample in the anode and cathode was uniform due to the application of vacuum pressure (Mahfouz 2013). Furthermore, the water content decreased dramatically from the initial high value of $188\% \pm 2\%$ in the EV series. To be specific, after the treatment the water content was 69% to 27.7% when the current density increased from 5A/$m^2$ to 15A/$m^2$, and the vacuum pressure increased from 30kPa to 50kPa.

### 3.4.4 Undrained Shear Strength

The shear strength of MFT samples after the tests was obtained by two methods. Because of the predominant dewatering effect, the unconfined compressive strength of samples in the EV series (E3V1, E3V2 and E3V3) with 15 A/$m^2$ current density could be measured directly by a pocket penetrometer (Model 29-3729). On the other hand, an empirical equation fitted for MFT-A (Guo and Shang 2014) was used to estimate the undrained shear strength for MFT-B. The correlation is shown as follow,

$$s_u = 104.83e^{-0.057w} \qquad [3.2]$$

Where $s_u$ (kPa) is the undrained shear strength, e (-) is the void ratio and w (%) is the water content.

Figs 3.12 (a) and (b) present the influence of current density and vacuum pressure on the undrained shear strength, respectively. As is shown in Fig 3.12 (a), the undrained shear strength increased linearly with the increase in the current density under the constant vacuum pressure. The undrained shear strength also increased

`

linearly with the increase in the vacuum pressure under the constant current density, as shown in Fig 3.12(b). Table 3.7 shows the results of the undrained shear strength from the penetrometer test and Fig 3.13 shows the results of the undrained shear strength versus water content. It can be seen that the result from the penetrometer test keeps consistent with that from the correlated equation for MFT-A from the vane shear test (Guo and Shang 2014). When the final water content reaches 53%, the undrained shear strength exceeds 5kPa. That is the minimum requirement for the treatment of MFT. The most significant strengthening effect was observed in the EV series tests. For example, in the E3V series with the combination of 15A/$m^2$ current density and 30kPa to 50kPa vacuum pressure, the undrained shear strength increased to the range of 12.3kPa to 24.5kPa. It was also observed that in the EV series, water in the cathode was discharged readily because of the application of the vacuum pressure. The final shear strength gain, therefore, was more uniform along the sample. On the other hand, the shear strength gain was the lowest in the S series with surcharge preloading due to the low surcharge loading applied. The undrained shear strength was in the range of 0.15 kPa to 0.2 kPa based on the correlation when surcharge loading of 1 kPa to 3 kPa was applied.

### 3.4.5 Atterberg Limits

The liquid limit and plastic limit of MFT near the anode and cathode were measured in the EK-vacuum cell before and after the tests following ASTM D4318 (2010). Originally, the liquid limit and plastic limit of MFT-B were 46.7% and 20.6%,

`

respectively. The results of Atterberg limits after the tests are summarized in Table 3.8 and the following is observed. 1) No significant increase in the plastic limit, as shown in Table 3.8. The plastic limit increased to 26% to 29% corresponding to 5 $A/m^2$ to 15 $A/m^2$ current density; 2) Considerable increase in the liquid limit, as shown in Table 3.8. The liquid limit after EK treatment ranged from 54.91% in E1 series to 64.4% in E3V3 series. They were much higher than the initial liquid limit of 46.7%. It has been reported that the increase in the liquid limit was the reflection of the electrochemical effect and soil cementation development (Indraratna and Hudson 2005). The samples prepared for the Atterberg limit tests were directly collected in the vicinity of the electrodes where the electrochemical reaction was intensive. The obvious increase in the liquid limit, therefore, could be observed. 3) No effect of vacuum pressure. The vacuum pressure has no effect on the increase in the liquid limit, as shown in Table 3.8.

The Casagrande's plasticity chart is plotted in Fig 3.14. The samples after E series, EV series and ES series were located above the A-line; hence MFT-B could be categorized as CH after these tests. In comparison, the original MFT was classified as CL (section 3.2.2). The results indicated that the plasticity of MFT increased after the EK treatment. It was attributed to the significantly increase in the liquid limit and relatively unchanged plastic limit. The similar result has been reported by other researchers (Dong et al 2009, Elazar 2011 and Guo and Shang 2014). The increase in the liquid limit and plasticity of MFT after the EK treatment is a positive dewatering and solidification result.

`

### 3.4.6 Power Consumption

In this thesis, the energy consumption by the vacuum pressure system is not considered. The power consumption of EK dewatering of MFT is defined as

$$E = \int \frac{UIdt}{v_M} \qquad [3.3]$$

Where E (kWh/$m^3$) is the energy consumption per cubic meters MFT treated, U (volt) is the voltage, I (A) is the current, t (h) is the time and $v_M$ ($m^3$) is the volume of MFT.

The power consumption in real time is plotted in Fig 3.15. The energy consumption in the test duration is summarized in Table 3.8. The duration of the single treatment (E series) and the combined EK and surcharge preloading treatment (ES series) was 48 hours. That in the EK and vacuum combined treatment (EV series) was 30 hours. As is shown in Fig 3.15, there was no difference in the initial power consumption in the E series and EV series (3.5kW/$m^3$) when t=0. However, under the constant current density, the increasing vacuum pressure led to the increase in the power consumption. For example, the peak power consumption was from 8.6 kW/$m^3$ to 10 kW/$m^3$ corresponding to the vacuum pressure from 30kPa to 50kPa under 15A/$m^2$ current density. This is attributed to the fact that the application of vacuum pressure makes the EK treatment more effective, i.e. more water discharged.

As is seen in Table 3.9, under the same current density, the power consumption in the EV series was higher than that in the E series. To be specific, the power

`

consumption in the EV series was 1.1 to 1.7 times higher than that in the E3 series with15 A/$m^2$ current density.

## 3.5 Summary

In this chapter, the characterization tests were conducted to obtain the physical and chemical properties of MFT-B. The EO permeability was also measured to assess the feasibility of EK dewatering treatment. The details of the EK-vacuum cell test were described. The experiments included five series, i.e. E series, S series, V series, EV series and ES series. The procedure of the EK-vacuum cell test was presented and the results of the combined effect of EK, vacuum and surcharge loading on the water flow, settlement, undrained shear strength, water content, power consumption and Atterberg limits were discussed. It was concluded that,

- The mature fine tailings (MFT) had high water content of 188% ± 2%. The specific gravity and initial void ratio of it was 2.49 and 4.68 respectively. A high content of organic matter (19.9%) and low carbonate content (<1%) could be observed. The main minerals of it were illite, kaolinite and quartz.

- The measured EO permeability in the EK cell test was from 2.77x$10^{-9}$ $m^2$/sV to 4.95x$10^{-9}$ $m^2$/sV. This range was higher than $10^{-9}$ $m^2$/sV and indicated the feasibility of EK treatment on the MFT.

- The EK-vacuum cell test was divided into two stages, i.e. the stage controlled by current density and the stage controlled by voltage.

`

- The EK and vacuum combined dewatering process (EV series) was the most effective in terms of significantly and uniformly decreases in water content and increases in undrained shear strength. The final undrained shear strength gained in the EV series exceeded 5kPa. The final settlement could reach 50% to 60% of the total height of the sample under the combined effect of 15 $A/m^2$ current density and 30kPa to 50kPa vacuum pressure.

- The final water content decreased linearly with the increasing current density and vacuum pressure.

- The final undrained shear strength increased linearly with the increasing current density and the vacuum pressure.

- The plastic limit of MFT did not significantly change, whereas a considerable increase in the liquid limit was observed after EK treatment.

- In the EV series, the increase in the vacuum pressure led to the increase in the power consumption under a constant current density.

`

Table 3.1 Physical Properties of Mature Fine Tailings

| parameters | MFT-A (Guo and Shang 2014) | MFT-B |
|---|---|---|
| Specific Gravity, Gs | 2.51 | 2.49 |
| Natural water content w (%) | 171.3 | $188 \pm 2$ |
| Void ratio, e | 4.39 | 4.68 |
| Dry density ($Mg/m^3$) | 0.47 | 0.44 |
| Liquid limit, LL(%) | 59.6 | 46.7 |
| Plastic limit, PL (%) | 29.1 | 20.6 |
| Plasticity index, $I_p$(%) | 22.5 | 26.1 |
| Natural pH of suspension | — | 7.55 |
| Carbonate content(%) | <1 | <1 |
| Organic matter(%) | 14.7 | 19.9 |
| D10 (μm) | 0.85 | 8 |
| D30 (μm) | 7.51 | 25 |
| D60 (μm) | — | 35 |
| D90 (μm) | 27.9 | 70 |
| Sand (%) | 0 | 7 |
| Clay (%) | 20 | 4 |
| Silt (%) | 80 | 89 |

`

Table 3.2 Major Cations Contained in Pore Water of MFT

| Cations | Concentrations (mg/L) | |
|---|---|---|
| | MFT-A (Guo and Shang 2014) | MFT-B |
| $Na^{+}$ | 599.55 | 590.12 |
| $Ca^{2+}$ | 9.68 | 9.45 |
| $Mg^{2+}$ | 9.03 | 28.45 |
| $K^{+}$ | 19.73 | 59.22 |
| $Al^{3+}$ | 0.04 | 0.01 |
| $Ba^{2+}$ | 0.10 | 0.55 |
| $Cu^{2+}$ | 0.11 | 0.65 |
| $Zn^{2+}$ | 0.01 | 0.25 |

Table 3.3 Result of Coefficient of EO Permeability

| Surcharge Loading (kPa) | J ($A/m^2$) | ke ($10^{-9}m^2/sV$) | |
|---|---|---|---|
| | | MFT-A (Guo and Sang 2014) | MFT-B |
| 3 | 5 | 10 | 2.77 |
| | 10 | 8 | 3.62 |
| | 15 | 14 | 4.95 |

Note: e=1.46

`

Table 3.4 Conditions of EK - Vacuum Cell Test (See Fig 3.5 to Fig 3.7)

| | E series | V series | S series | EV series | ES series |
|---|---|---|---|---|---|
| **Test No.** | E1 | V1 | S1 | E1V1 E1V2 E1V3 | E1S1 |
| | E2 | V2 | S2 | E2V1 E2V2 E2V3 | E1S2 |
| | E3 | V3 | | E3V1 E3V2 E3V3 | E2S1 |
| | | | | | E2S2 |
| | | | | | E3S1 |
| | | | | | E3S2 |
| **Test Procedure** | EK dewatering applied alone | Vacuum pressure applied alone | Surcharge pressure applied alone | Vacuum pressure and EK dewatering applied simultaneously | Surcharge pressure and EK dewatering applied simultaneously |
| **Sample Height** | 65 mm | | | | |
| **Drainage Path** | Vertical | | | | |
| **Testing Time** | 12 hrs, 48 hrs | | | | |
| **Maximum Voltage Gradient** | 500V/m | | | | |
| **Current Density,J** | $5A/m^2$, $10A/m^2$, $15A/m^2$ | | | | |
| **Applied Surcharge Loading** | 1kPa, 3kPa | | | | |
| **Applied Vacuum Pressure** | 30kPa, 40 kPa, 50 kPa | | | | |
| **w% Test Location** | Anode & Cathode | | | | |
| **Electrodes** **Configuration** | Horizontal | | | | |
| **Material** | Electrodes SS316 mesh | | | | |

`

Table 3.5 Detailed Information of Test Series

| Series | Test No. | $p_v$ kPa | J $A/m^2$ | $\sigma_v$ kPa |
|---|---|---|---|---|
| E | E1 | — | 5 | — |
| | E2 | — | 10 | — |
| | E3 | — | 15 | — |
| V | V1 | 30 | — | — |
| | V2 | 40 | — | — |
| | V3 | 50 | — | — |
| S | S1 | — | — | 1 |
| | S2 | — | — | 3 |
| EV | E1V1 | 30 | 5 | — |
| | E1V2 | 40 | 5 | — |
| | E1V3 | 50 | 5 | — |
| | E2V1 | 30 | 10 | — |
| | E2V2 | 40 | 10 | — |
| | E2V3 | 50 | 10 | — |
| | E3V1 | 30 | 15 | — |
| | E3V2 | 40 | 15 | — |
| | E3V3 | 50 | 15 | — |
| ES | E1S1 | — | 5 | 1 |
| | E1S2 | — | 5 | 3 |
| | E2S1 | — | 10 | 1 |
| | E2S2 | — | 10 | 3 |
| | E3S1 | — | 15 | 1 |
| | E3S2 | — | 15 | 3 |

Note:

1. Original water content, w%=188%± 2%
2. Original undrained shear strength, $s_u$=0kPa
3. Capacity of vacuum line is 67.7kPa.
4. Power consumption is electricity consumption

`

Table 3.6 Summary of Water Content

| Test Series | Water Content | |
|---|---|---|
| | Anode | Cathode |
| E1 | 91 | 147.2 |
| E2 | 81 | 120.9 |
| E3 | 71 | 116.6 |
| V1 | 88.4 | — |
| V2 | 77.7 | — |
| V3 | 71.4 | — |
| S1 | 115.3 | — |
| S2 | 109.7 | — |
| E1V1 | 69 | 119 |
| E1V2 | 52 | 91.5 |
| E1V3 | 48 | 71 |
| E2V1 | 49 | 66.9 |
| E2V2 | 44 | 60.5 |
| E2V3 | 35.9 | 49.8 |
| E3V1 | 37.4 | — |
| E3V2 | 34.9 | — |
| E3V3 | 27.7 | — |
| E1S1 | 88.5 | 144 |
| E1S2 | 83.9 | 143 |
| E2S1 | 78.5 | 128.3 |
| E2S2 | 74.5 | 127 |
| E3S1 | 68.5 | 108.2 |
| E3S2 | 65.3 | 106.6 |

Table 3.7 Summary of Undrained Shear Strength

| Test Series | Undrained Shear Strength, $s_u$ (kPa) | |
|---|---|---|
| | From Penetrometer Test | From Correlated Equation (Eq [3.2]) (Guo and Shang 2014) |
| E3V1 | 12.3 | 12.4 |
| E3V2 | 14.7 | 14.3 |
| E3V3 | 24.5 | 21.6 |

`

Table 3.8 Summary of Atterberg Limits

| Test No. | Atterberg Limit | | | | | |
|---|---|---|---|---|---|---|
| | Anode | | | Cathode | | |
| Series | LL | PL | PI | LL | PL | PI |
| E1 | 56.29 | 22.54 | 33.75 | 54.61 | 20.56 | 34.05 |
| E2 | 54.91 | 21.08 | 33.83 | 92.30 | 176.10 | 189.10 |
| E3 | 58.42 | 24.93 | 33.49 | 55.10 | 21.46 | 33.64 |
| E1V1 | 60.23 | 26.55 | 33.68 | — | — | — |
| E1V2 | 61.79 | 27.00 | 34.79 | — | — | — |
| E1V3 | 61.60 | 28.25 | 33.35 | — | — | — |
| E2V1 | 56.00 | 26.00 | 30.00 | — | — | — |
| E2V2 | 61.80 | 27.75 | 34.05 | — | — | — |
| E2V3 | 60.23 | 29.46 | 30.77 | — | — | — |
| E3V1 | 60.30 | 27.00 | 33.30 | — | — | — |
| E3V2 | 64.14 | 27.13 | 37.01 | — | — | — |
| E3V3 | 64.40 | 29.25 | 35.15 | — | — | — |
| E1S1 | 57.40 | 23.97 | 33.43 | 55.23 | 20.80 | 34.43 |
| E1S2 | 58.10 | 24.89 | 33.21 | 55.80 | 20.88 | 34.92 |
| E2S1 | 58.60 | 24.14 | 34.46 | 55.40 | 21.00 | 34.40 |
| E2S2 | 59.27 | 24.18 | 35.09 | 55.15 | 21.58 | 33.57 |
| E3S1 | 59.40 | 25.55 | 33.85 | 54.48 | 21.57 | 32.91 |
| E3S2 | 61.70 | 25.89 | 35.81 | 56.13 | 21.79 | 34.34 |

`

Table 3.9 Summary of Power Consumption

| Test Series | Power Consumption ($kWh/m^3$) |
|---|---|
| E1 | 40.1 |
| E2 | 48.4 |
| E3 | 72 |
| E1V1 | 51.3 |
| E1V2 | 55.6 |
| E1V3 | 57 |
| E2V1 | 60.7 |
| E2V2 | 65.3 |
| E2V3 | 73.3 |
| E3V1 | 80.1 |
| E3V2 | 111.2 |
| E3V3 | 124.7 |
| E1S1 | 50.1 |
| E1S2 | 51.5 |
| E2S1 | 50.5 |
| E2S2 | 52.7 |
| E3S1 | 75.1 |
| E3S2 | 79.6 |

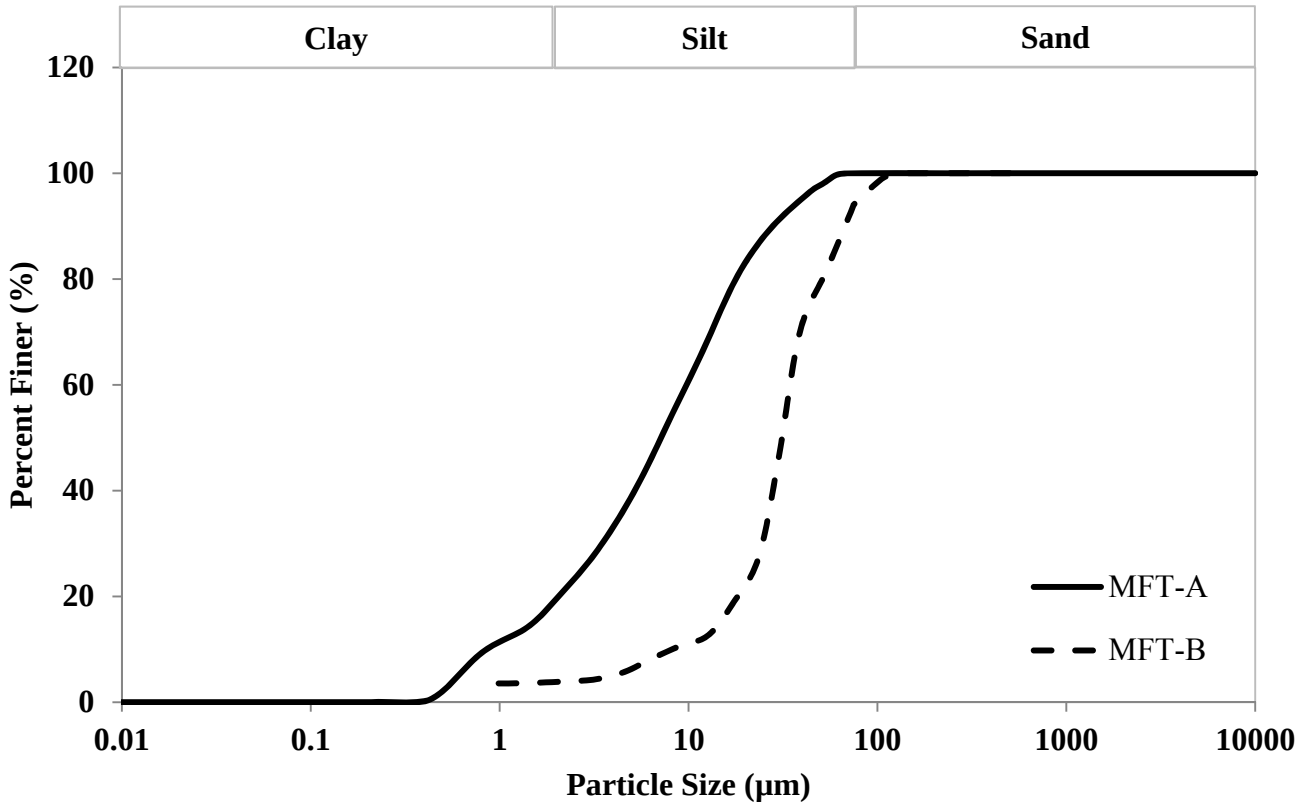


Fig 3.1 Grain Size Distribution of MFT

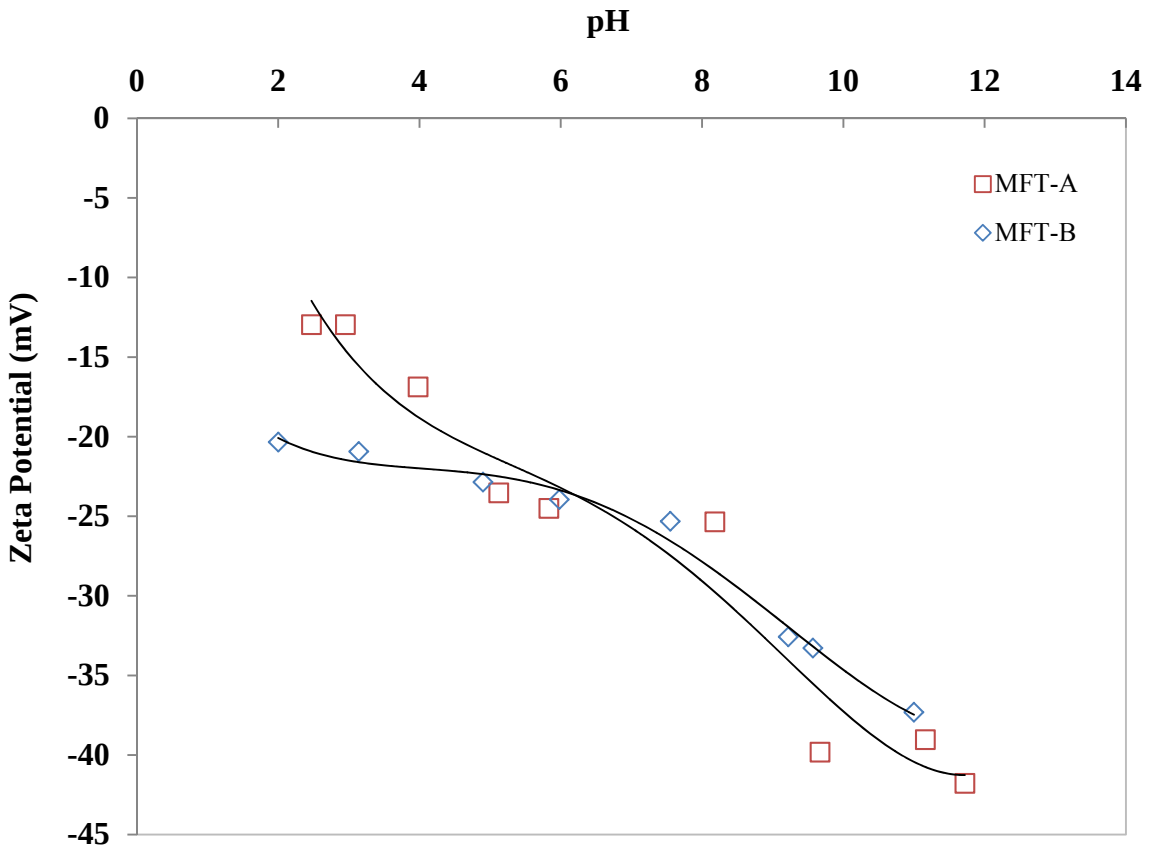


Fig 3.2 Zeta potential VS pH of Mature Fine Tailings Suspensions

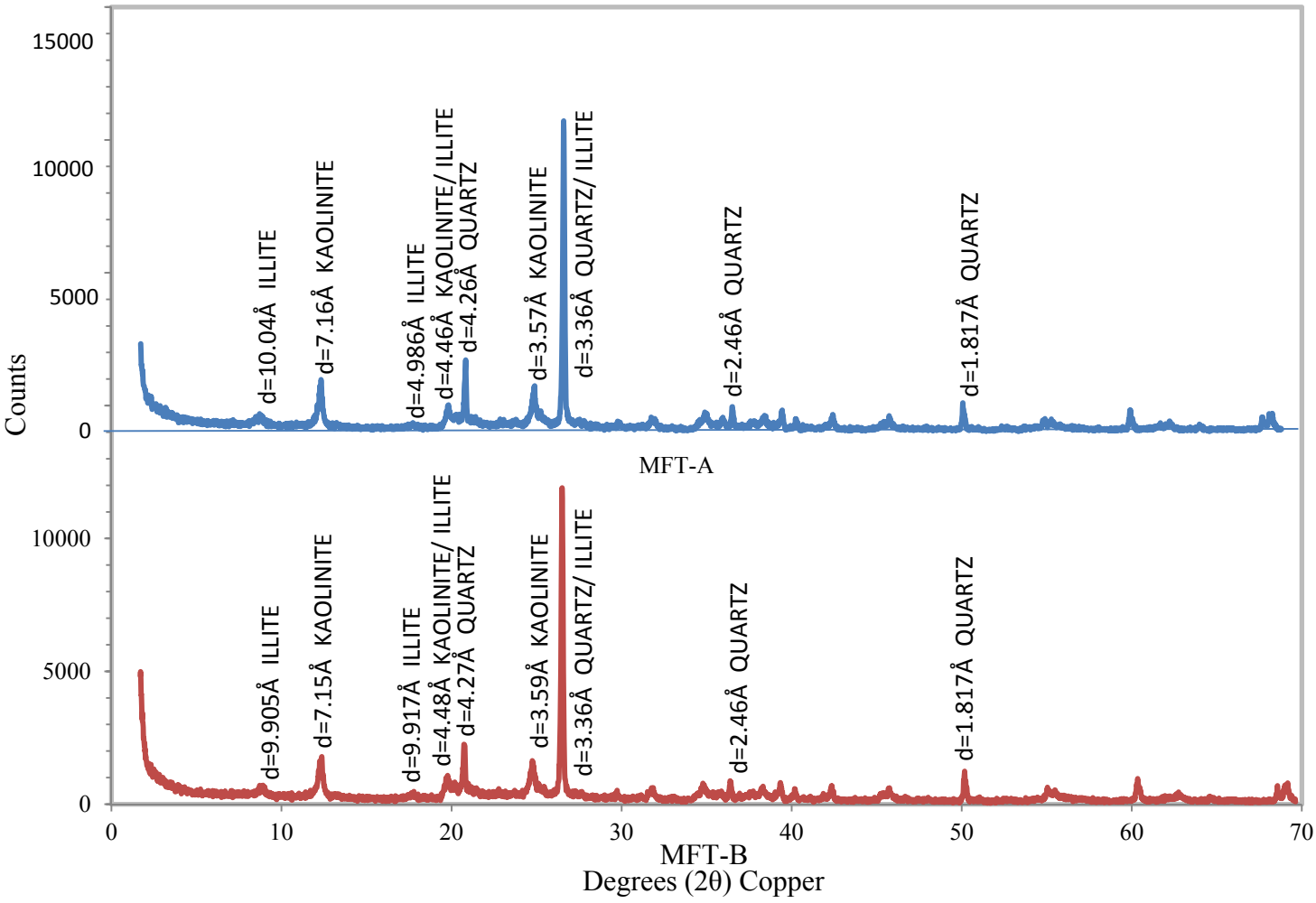


Fig 3.3 X-ray Diffraction on Bulk Sample of Mature Fine Tailings

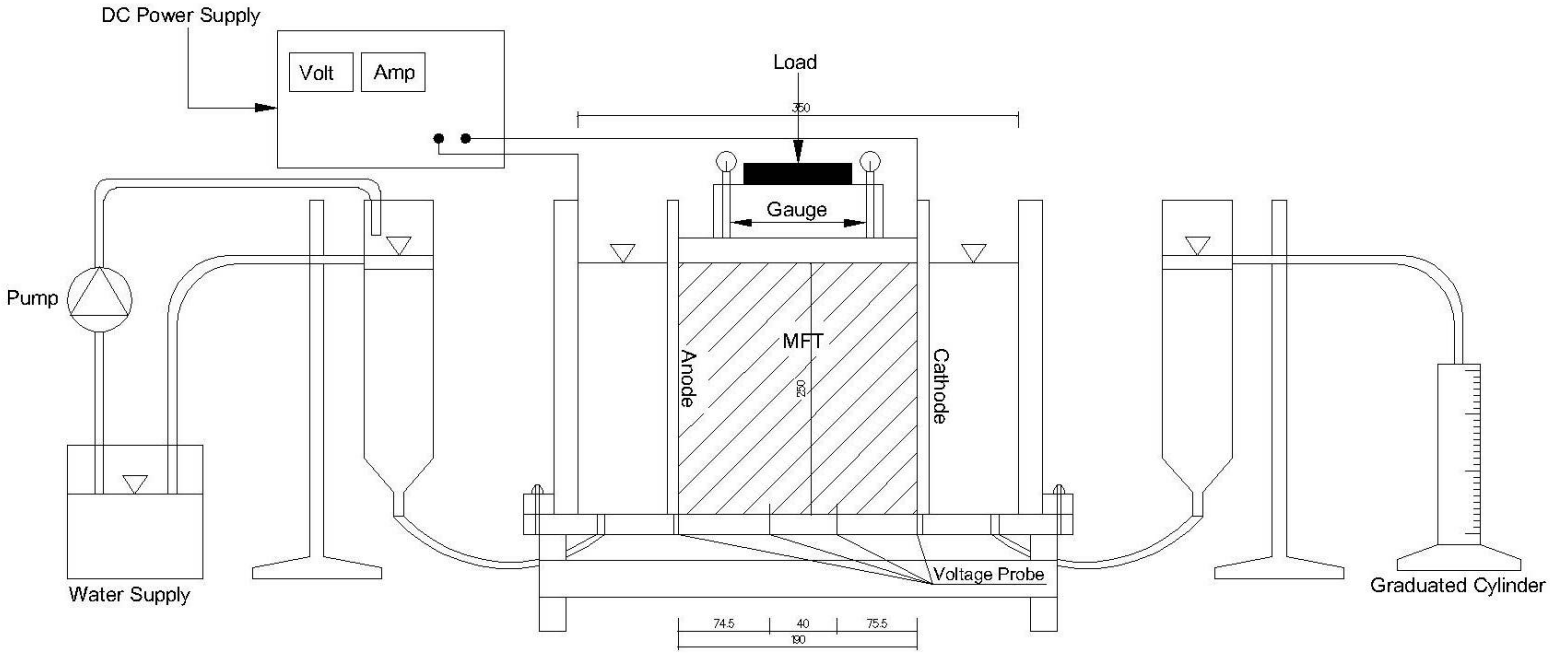


Fig 3.4 Schematic of EK Cell Test (Redrawn from Guo and Shang 2014)

`

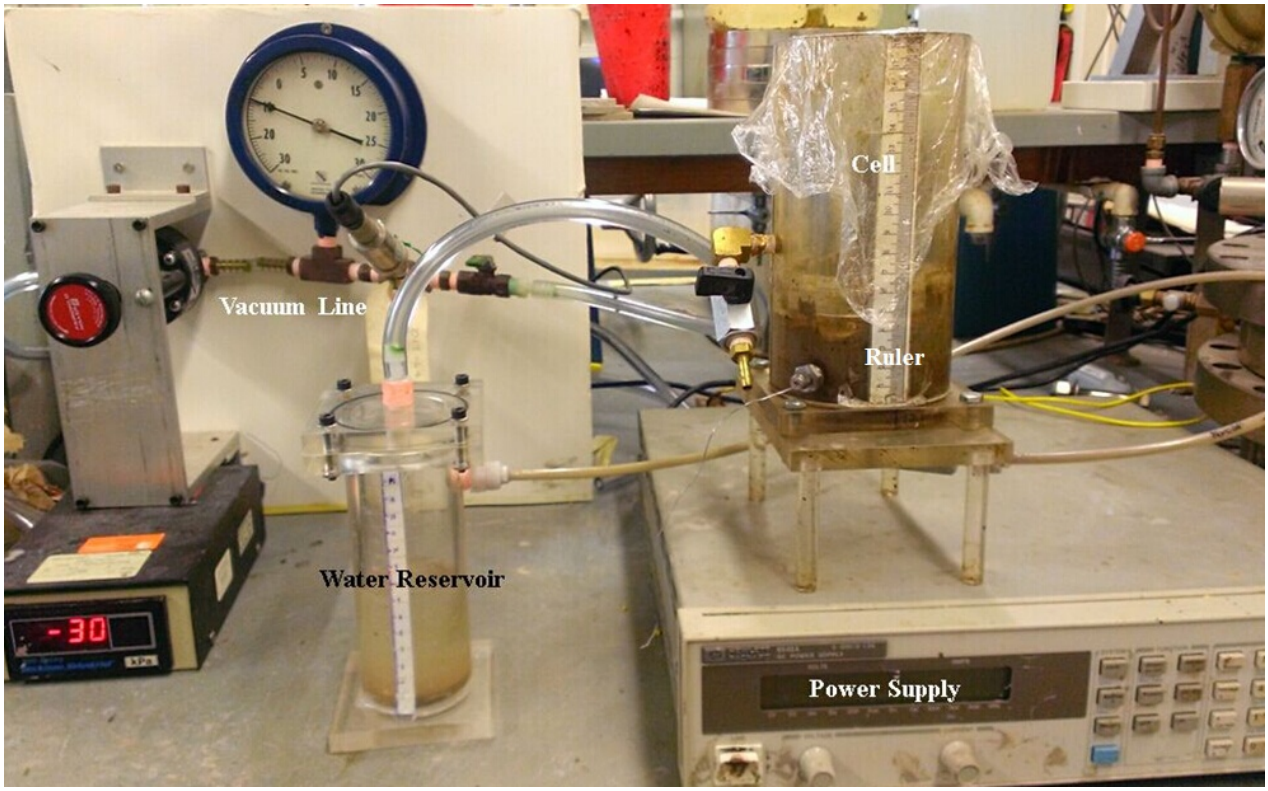


Fig 3.5 EK-vacuum Cell Setup

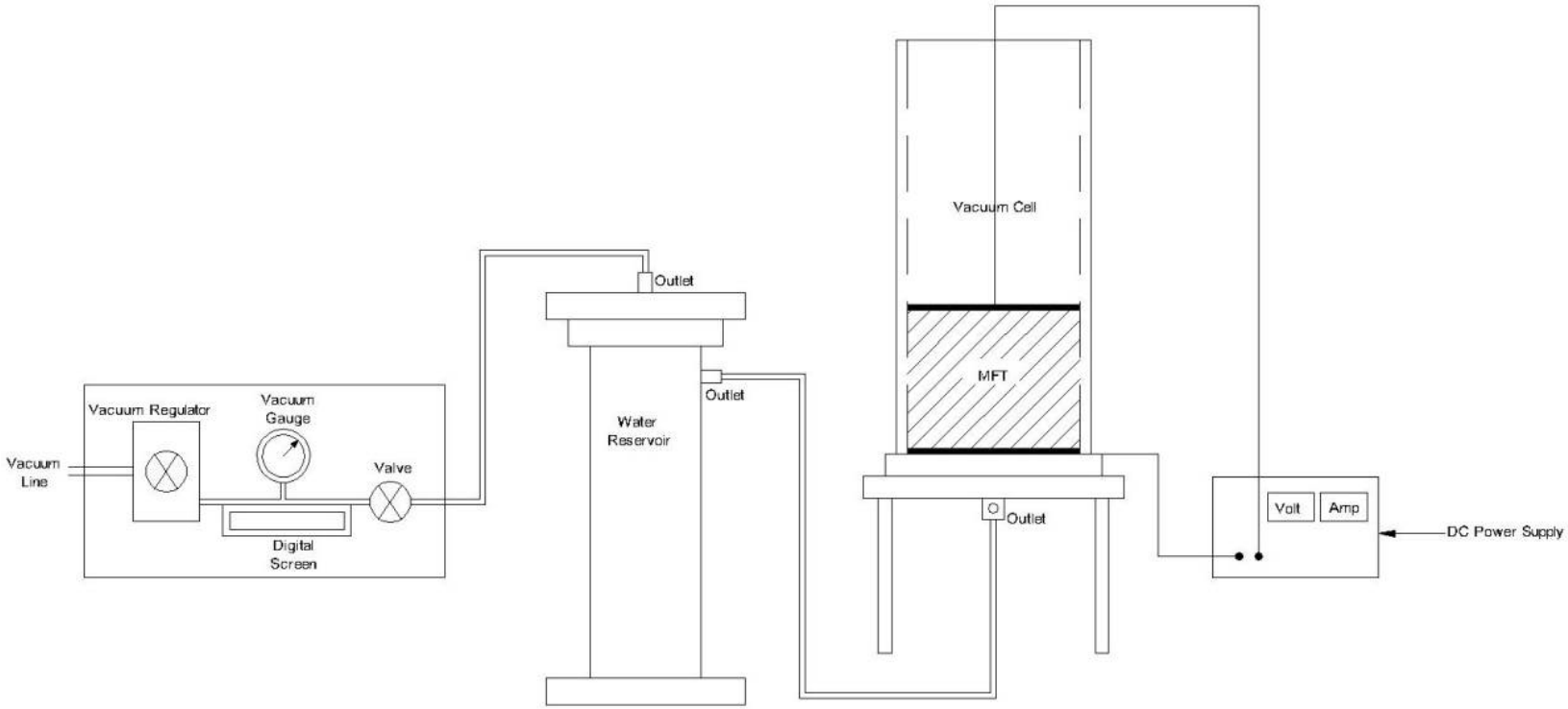


Fig 3.6 Schematic of EK - vacuum Cell Test

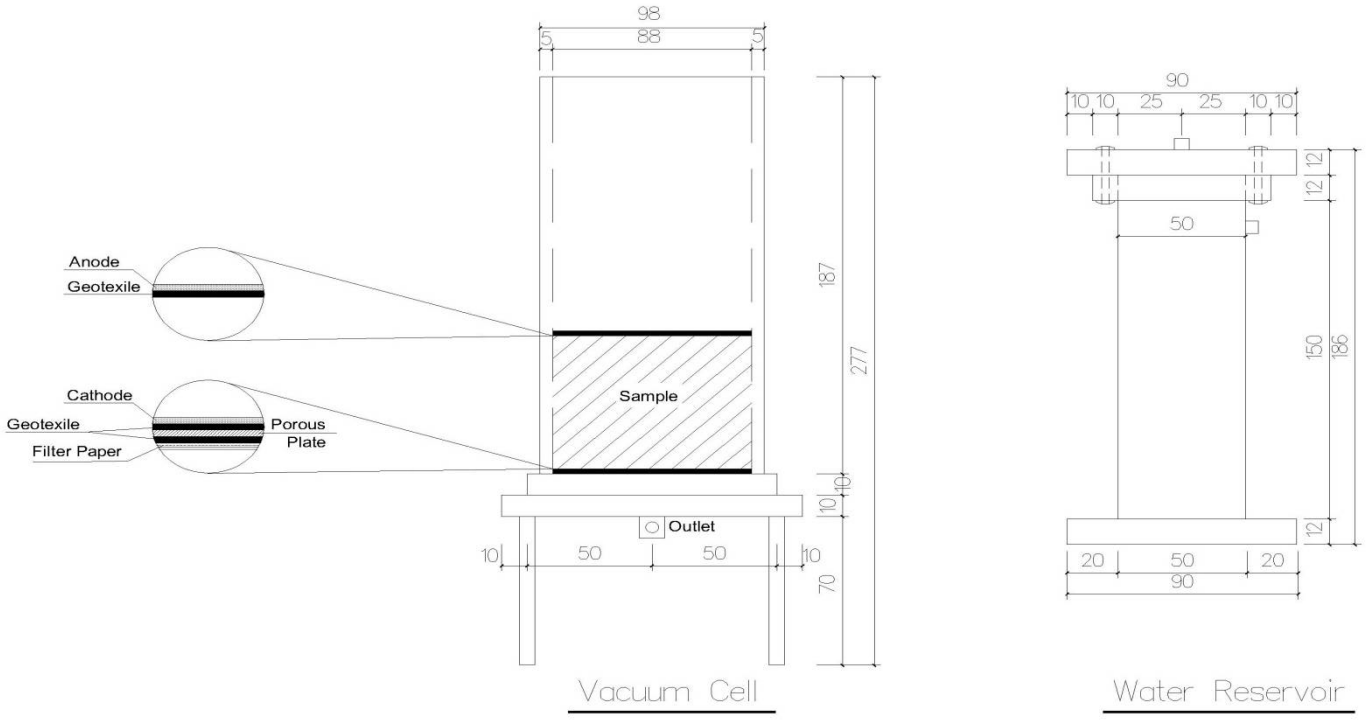


Fig 3.7 Detailed Drawing of EK-Vacuum Cell

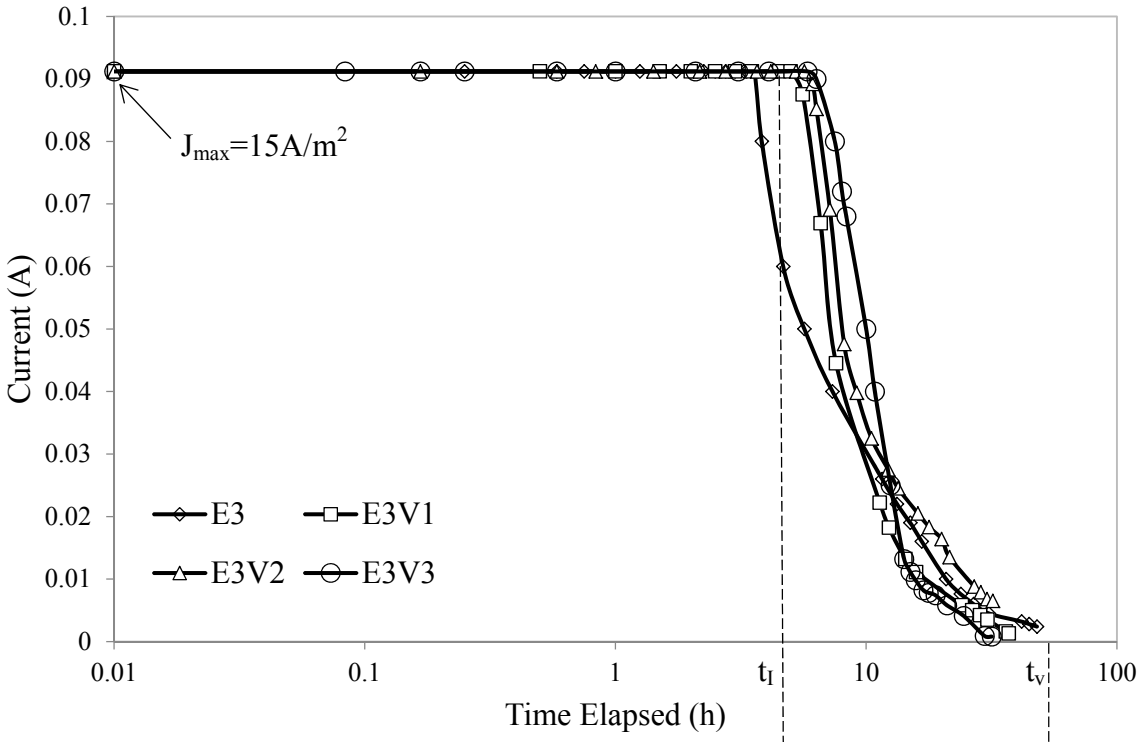


(a)

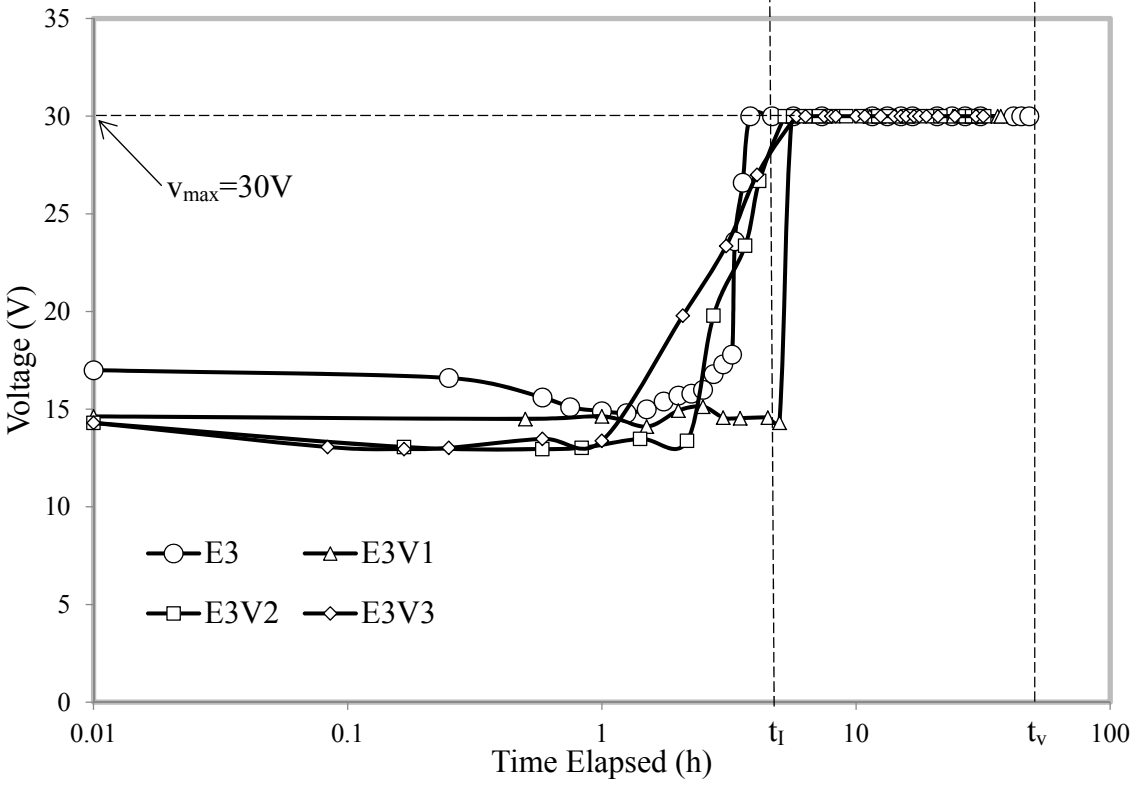


(b)

Fig 3.8 (a) Voltage vs Time (b) Current vs Time

Note: $t_I$ is the time during which current control and $t_v$ is the time during which voltage control

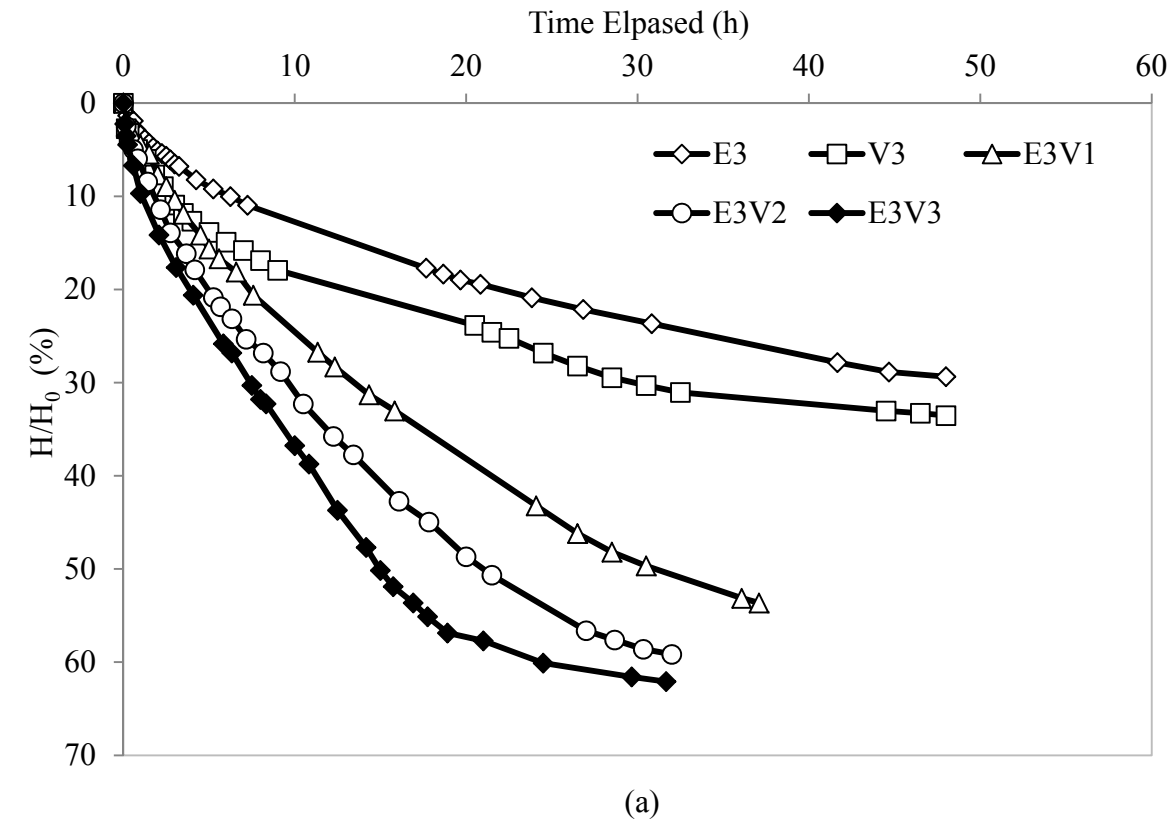


(a)

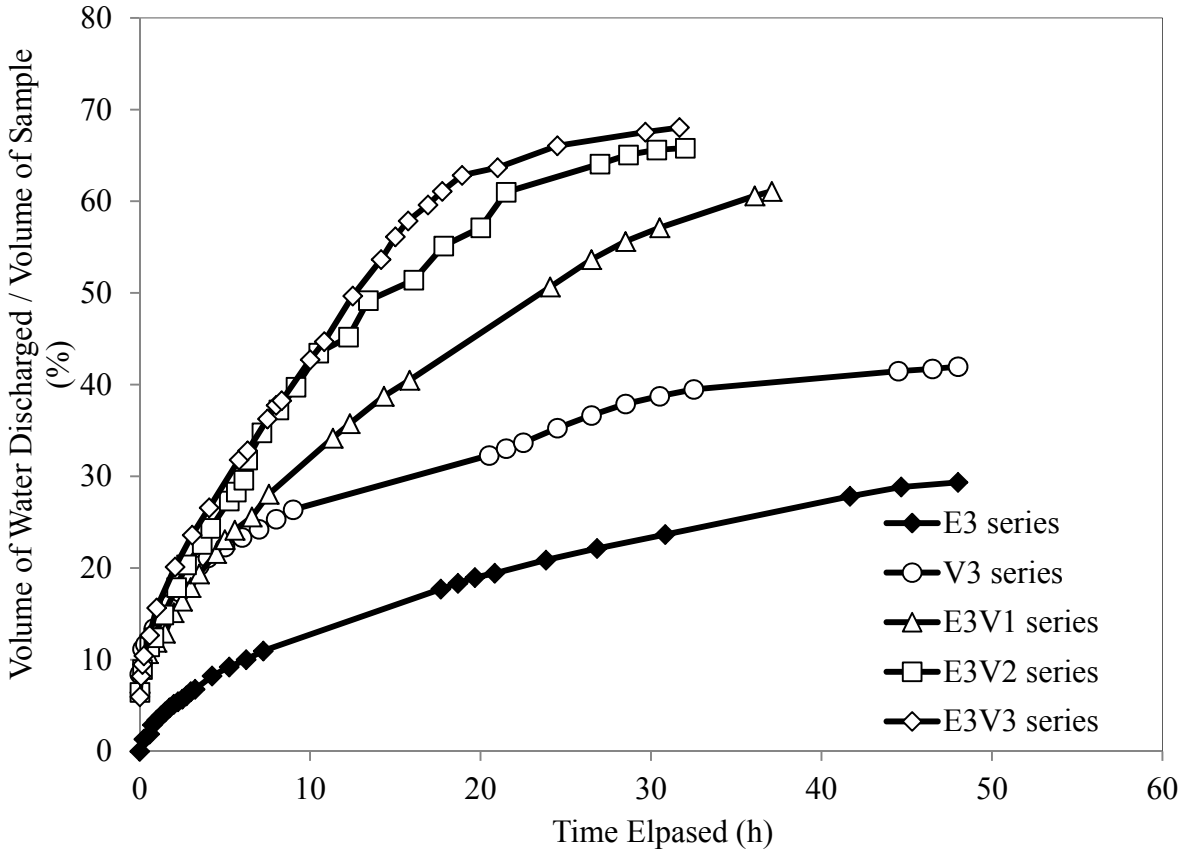


(b)

Fig 3.9 (a) Normalized Settlement vs Time (b) Normalized Water Discharged vs Time

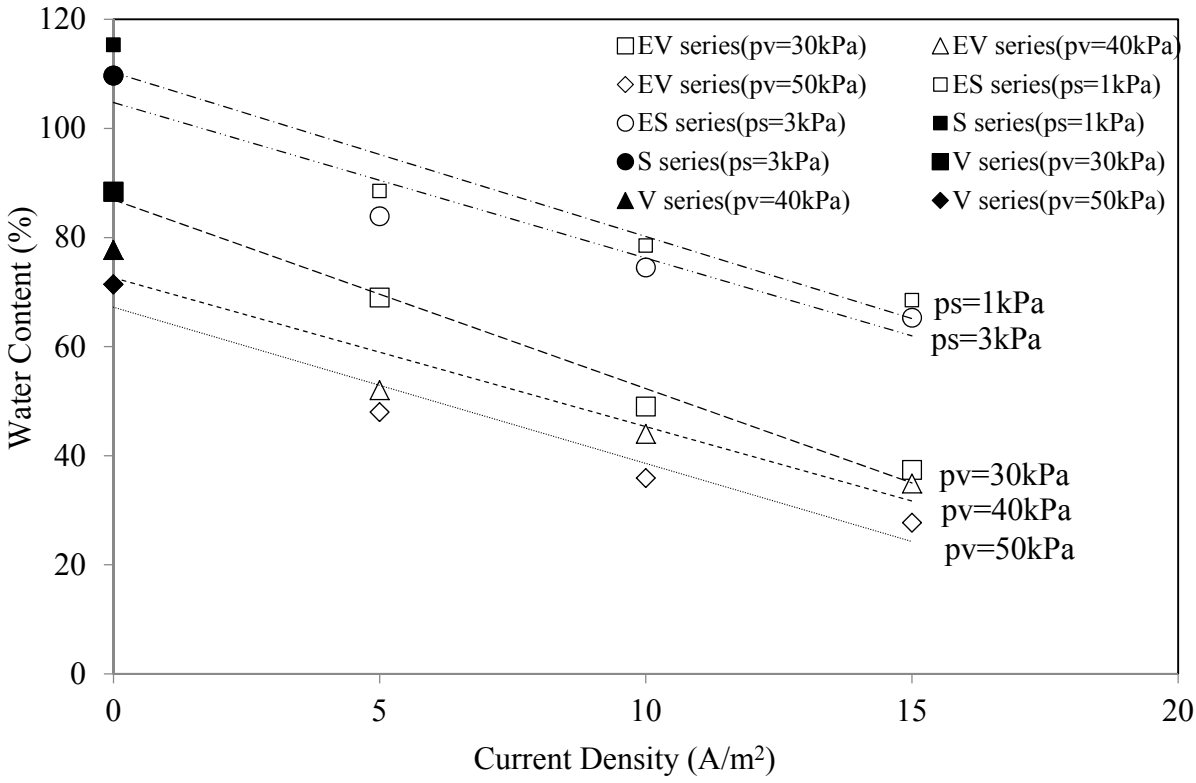


(a)

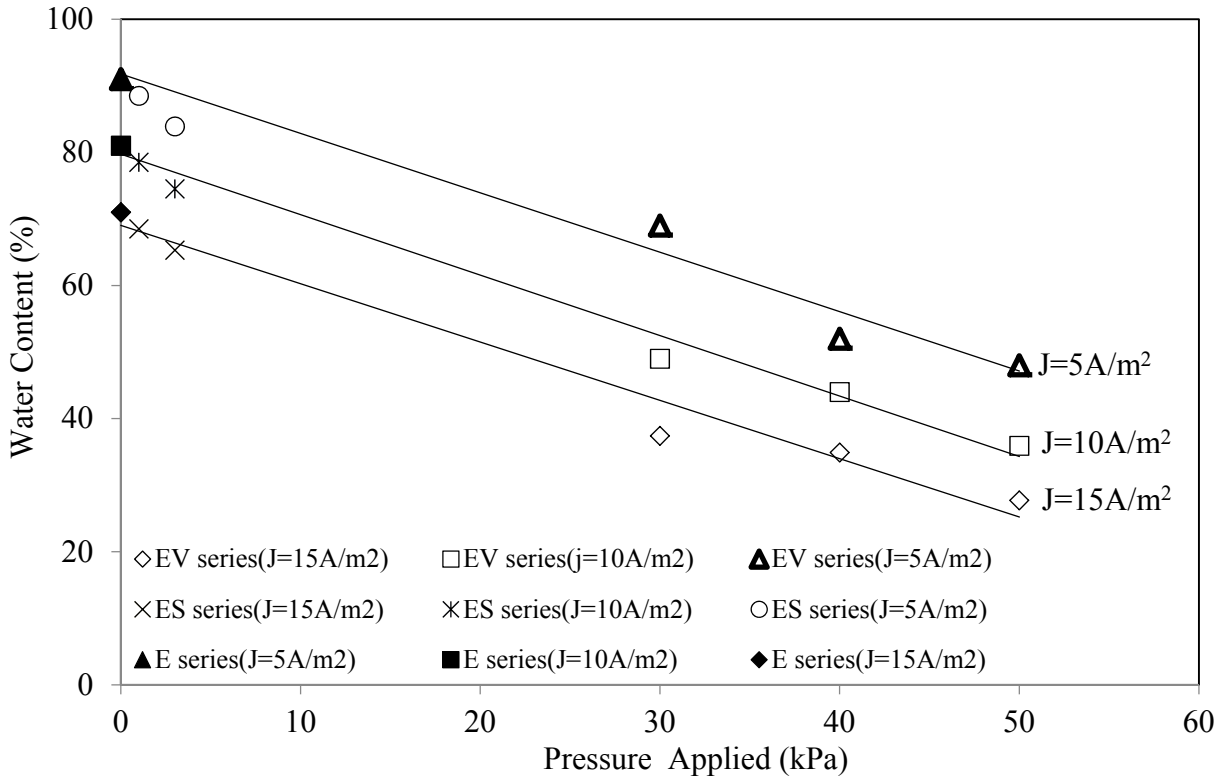


(b)

Fig 3.10 (a) Current Density vs Water Content (b) Pressure Applied vs Water Content

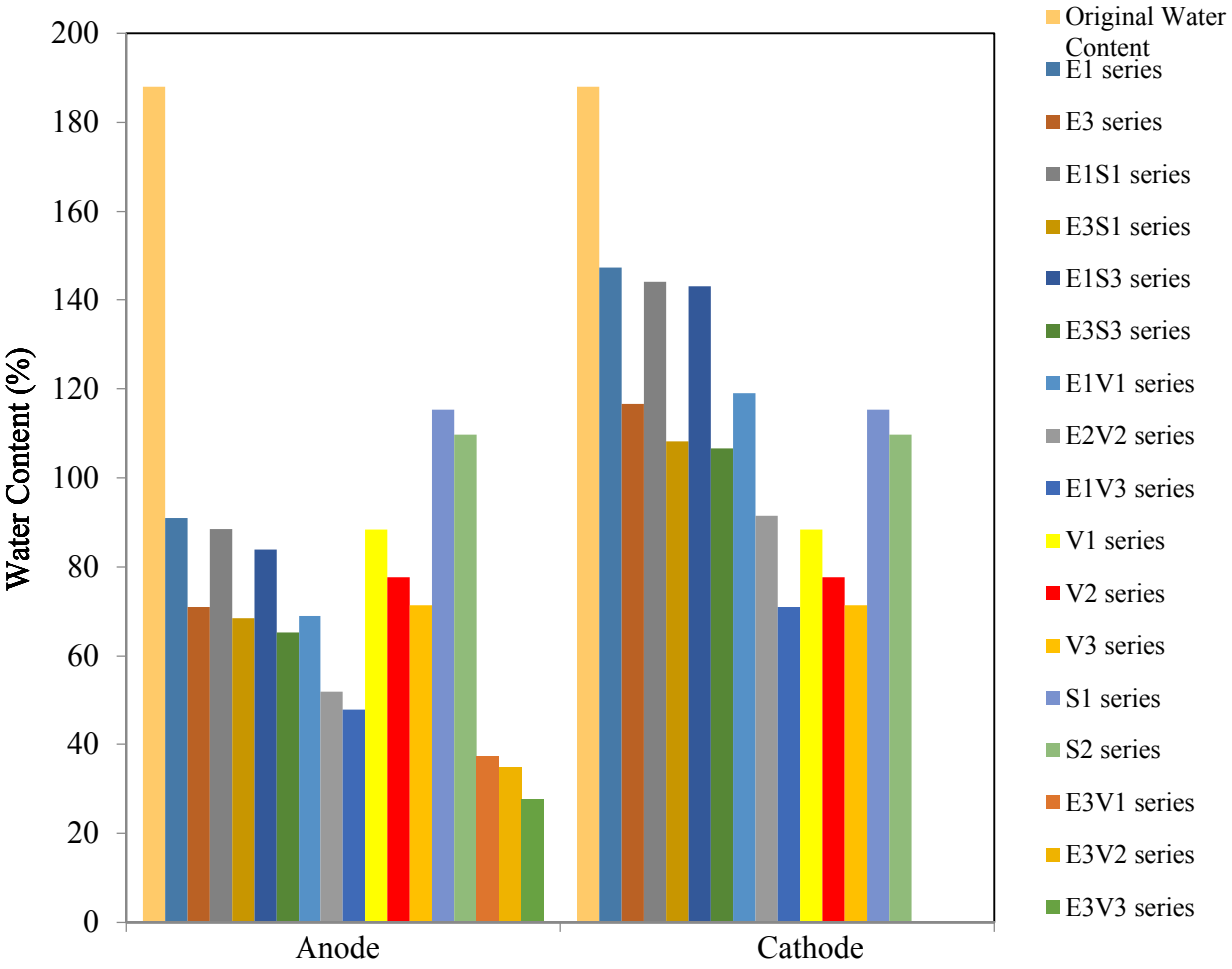


Fig 3.11 Water Content Before and After the Test Series

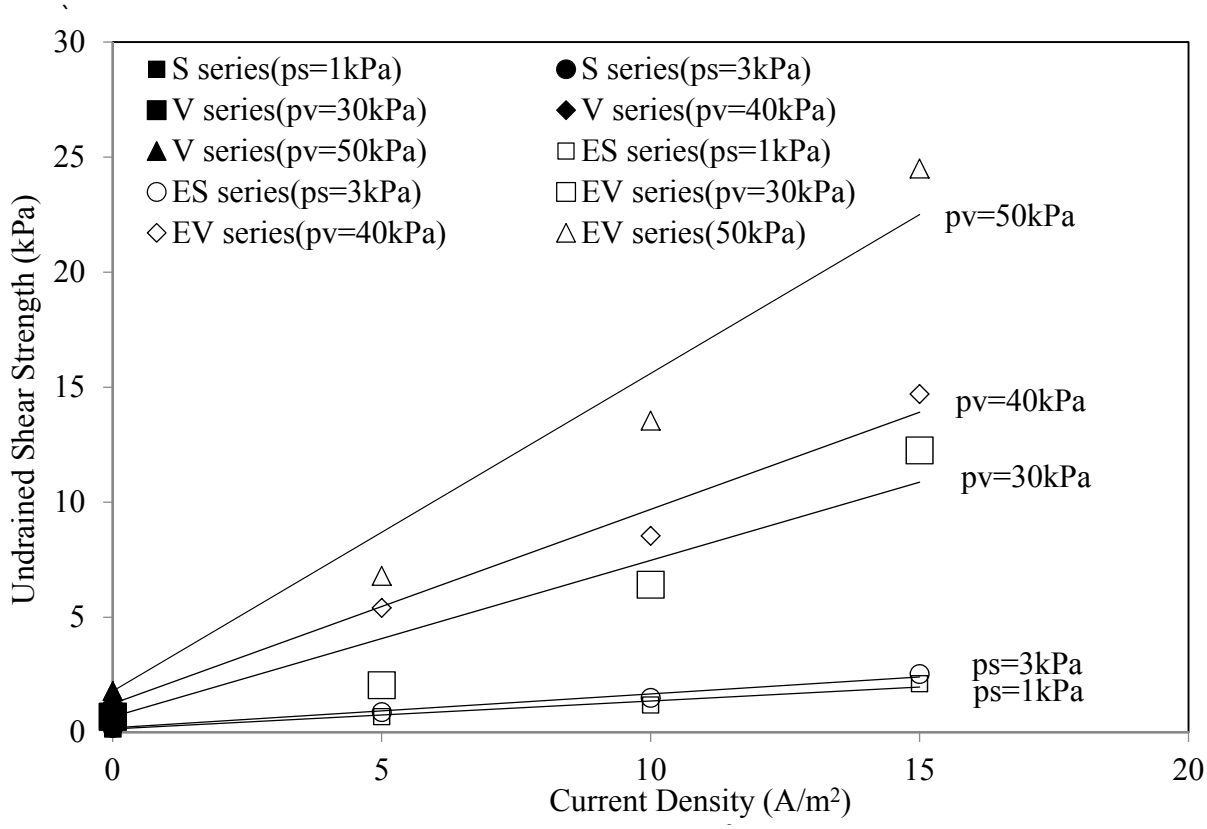


(a)

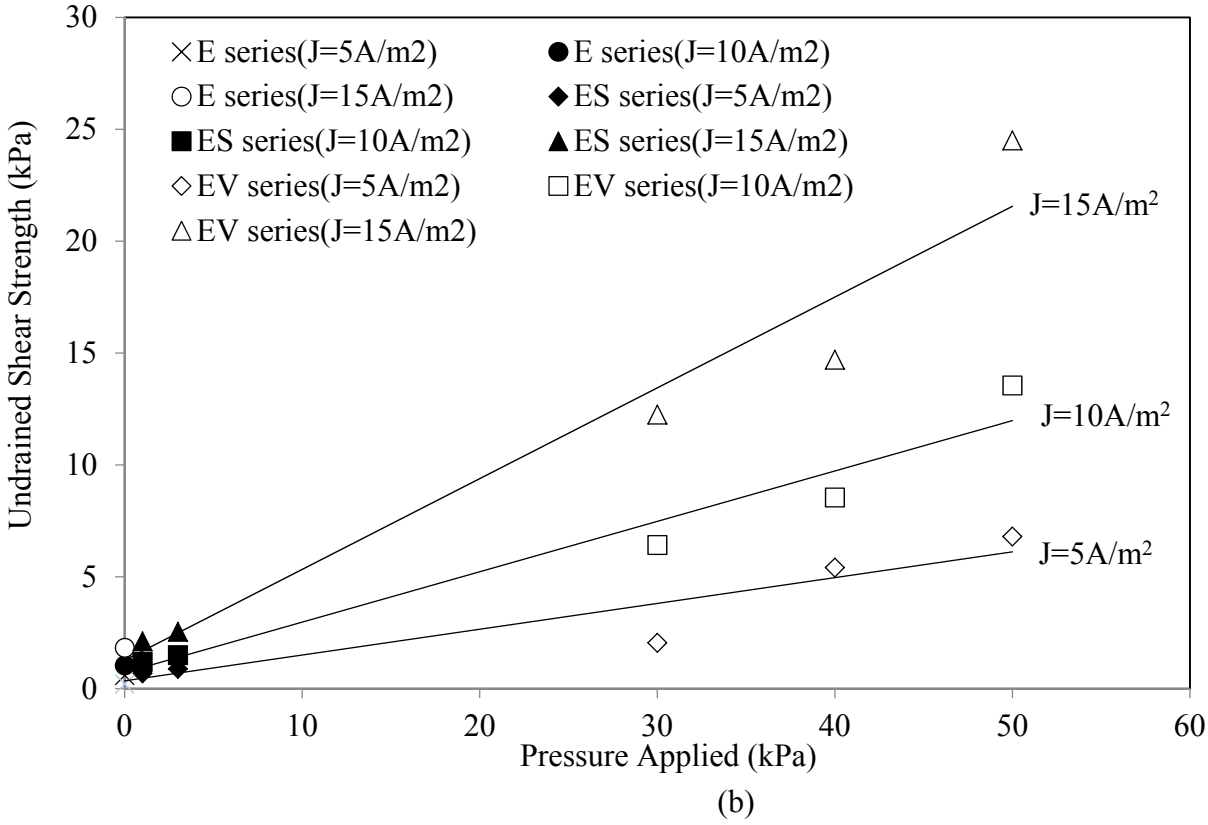


(b)

Fig 3.12 (a) Pressure Applied vs Undrained Shear Strength (b) Current Density vs Undrained Shear Strength

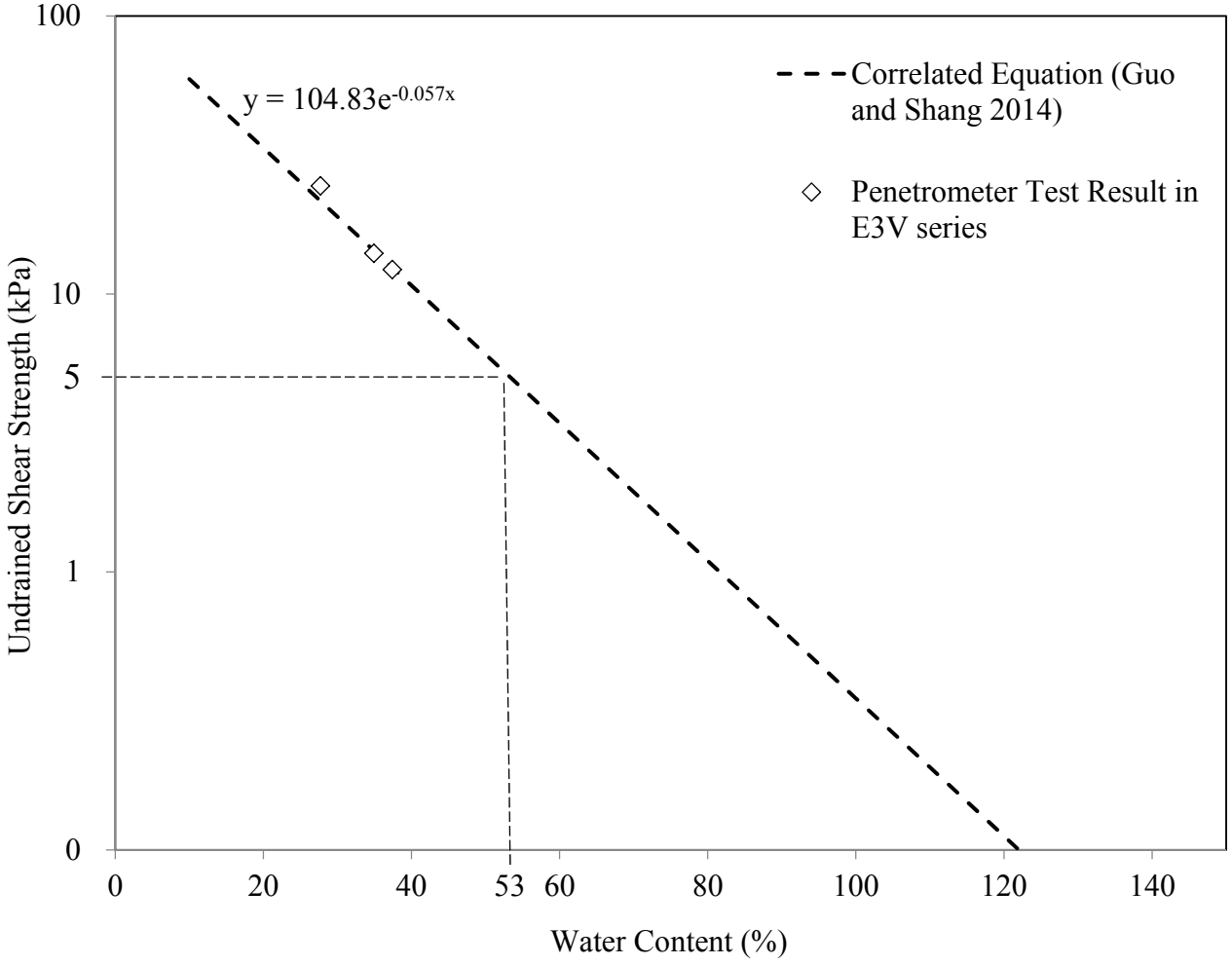


Fig 3.13 Undrained Shear Strength VS Water Content

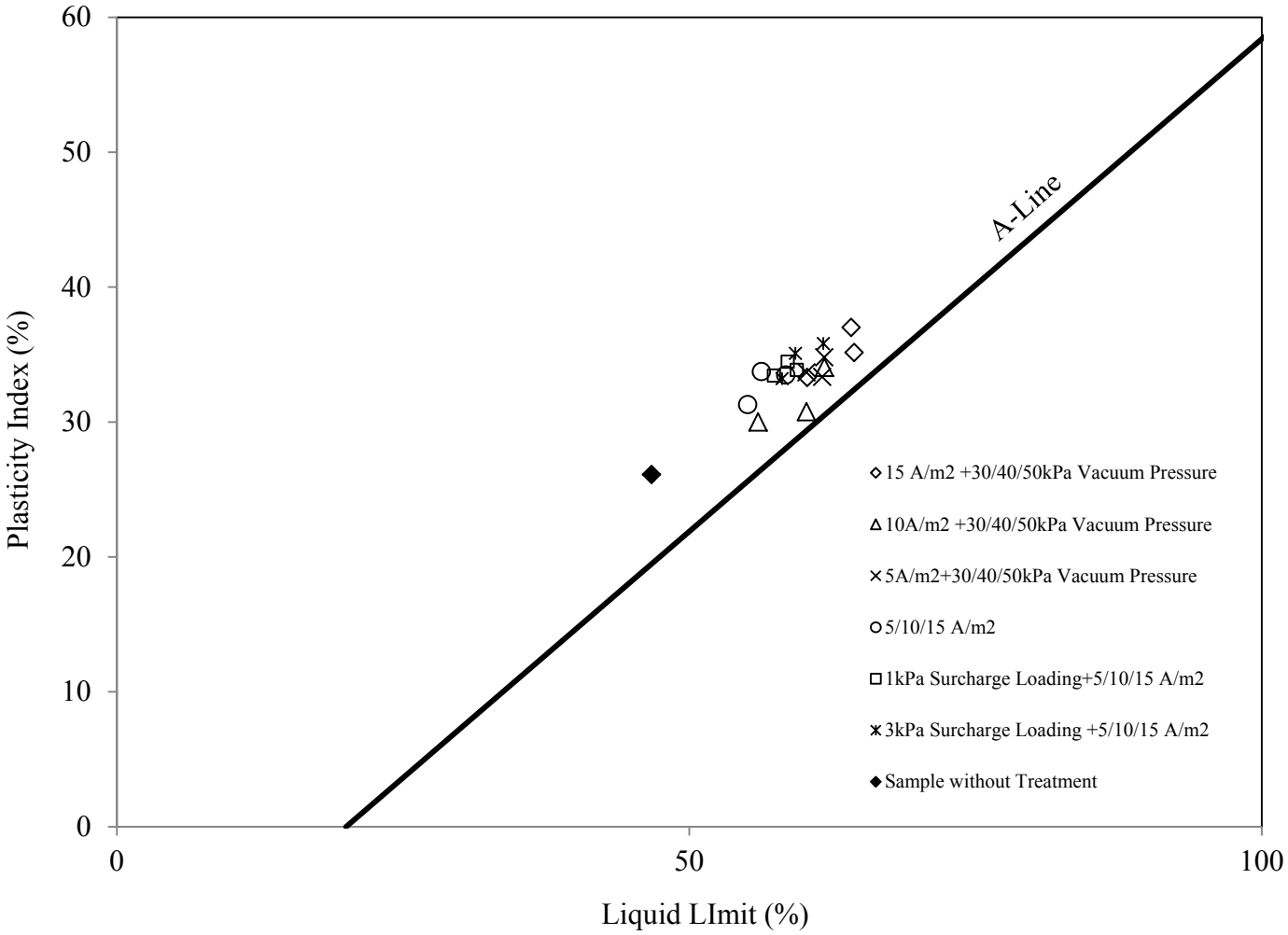


Fig 3.14 Plasticity Chart

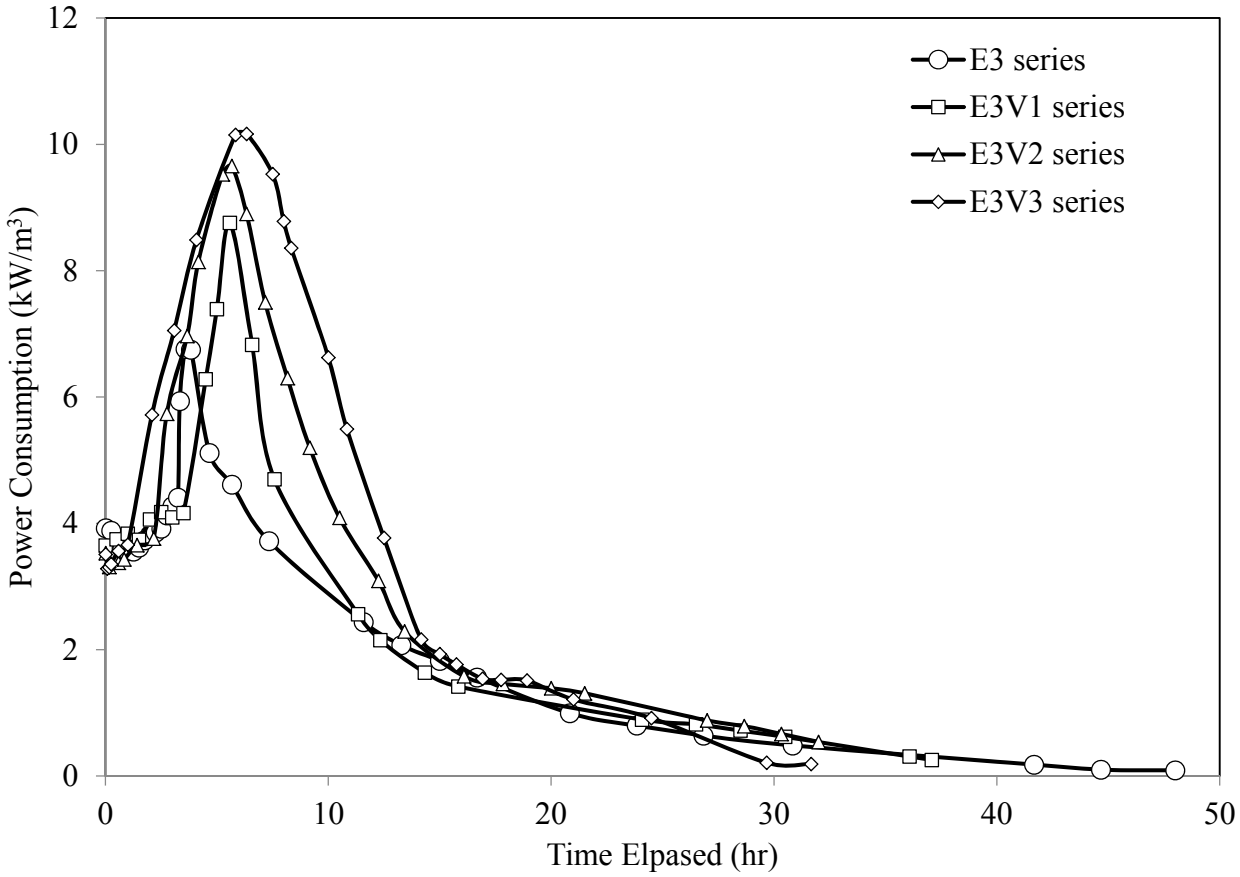


Fig 3.15 Power Consumption vs Time

`

# CHAPTER 4 THEORETICAL MODELING

## 4.1 Objective

An analytical model for one-dimensional consolidation by surcharge loading, vacuum pressure and EK treatment is developed in this chapter. The time-dependent pore water pressure and settlement are analyzed based on the model. As is shown in Fig 4.1, the boundary condition of the model is specified as that the vacuum pressure is applied at the bottom of the cell where the cathode is located. In this configuration, the drainage by gravity, surcharge loading, electroosmosis and vacuum pressure is in the same downward direction. The result of the analytical model is compared with that from experiments for verification and validation.

## 4.2 Assumptions

The assumptions made in the development of the model are as follows,

- The soil is homogeneous and fully saturated.
- The soil self-weight consolidation is negligible;
- The coefficient of consolidation ($c_v$) is constant during consolidation process;
- The movement of solids induced by the hydraulic flow and electrophoresis is negligible;
- Physical-chemical reactions generated by electrochemical reactions in the soil

`

and the vicinity of electrodes are ignored;

- The interaction between the vacuum pressure and electroosmosis is negligible.

## 4.3 One Dimensional Model for Combined Surcharge, Vacuum Pressure and EK Consolidation (EVS model)

The EVS model simulates the excess pore water pressure in a soil matrix generated by the vacuum pressure, surcharge pressure and electroosmotic pressure. The effects are represented by the changes of the pore water pressure in the soil. The final results of the analytical model are the linear superposition of the excess pore pressured generated by the vacuum pressure, surcharge preloading and electroosmosis.

## 4.4 Governing Equations and Solution

The expression of the excess pore water pressure can be described as the linear superposition of three components to evaluate the combined effect of the surcharge preloading, vacuum preloading and EK consolidation. The expression is shown as below.

$$u = u_q + u_v + u_{ek} \qquad [4.5]$$

Where u (kPa) is the total excess pore water, $u_q$ (kPa) is the excess pore water due to surcharge loading, $u_v$ (kPa) is the excess pore water due to vacuum pressure and $u_{ek}$ (kPa) is the excess pore water due to EK treatment.

`

The flow sheet of the solution is shown in Fig 4.2.

The solution of excess pore water pressure due to surcharge loading is derived from Terzaghi theory (Holtz and Kovacs 1981 and Elazar 2011),

$$u_q = q\sum_{n=0}^{\infty}\left(\frac{4}{(2n+1)\pi}\sin\frac{(2n+1)\pi z}{2h}\right)\exp\left(-\frac{(2n+1)^2\pi^2 T_v}{4}\right) \quad [4.1]$$

Where q (kPa) is the surcharge loading, z(m) is the depth, h (m) is the maximum drainage path and $T_v$ (-) is the time factor,

$$T_v = \frac{c_v \cdot t}{h^2} \quad [4.2]$$

Where $c_v$ ($m^2/s$) is the coefficient of consolidation and t(s) is the time.

The solution of the excess pore water pressure generated by vacuum pressure based on the given boundary condition and initial condition has been obtained as below (Mohamedelhassan 2002 and Chai and Carter 2013).

$$u_v = p_v\{1-\sum_{n=0}^{\infty}\left(\frac{4}{(2n+1)\pi}\sin\frac{(2n+1)\pi z}{2h}\right)\exp\left(-\left(\frac{2n+1}{2}\right)^2\pi^2 T_v\right) \quad [4.3]$$

Where $p_v$ (kPa) is the vacuum pressure, z(m) is the depth, h (m) is the maximum drainage path and $T_v$ (-) is the time factor.

The solution of excess pore water pressure due to EK treatment is based on the condition of closed anode and open cathode. It was developed by Esrig (1968) and

`

expressed as below,

$$u_{ek} = -\eta \frac{k_e}{k_h} \gamma_w U(x) + \eta \frac{2k_e \gamma_w U_m}{k_h \pi^2} \sum_{n=0}^{\infty} \frac{(-1)^n}{(n+\frac{1}{2})^2} \sin \frac{(n+\frac{1}{2})\pi z}{2h} [\exp(-(n+\frac{1}{2})^2 \pi^2 T_v)] \quad [4.4]$$

Where $k_e$ ($m^2$/sV) is the coefficient of electroosmotic permeability, $k_h$ (m/s) is the hydraulic conductivity, $\gamma_w$ (9.8 kN/$m^3$) is the unit weight of water, U(x) (V) is the voltage at distance x from the cathode, $U_m$ (V) is the maximum voltage at anode, z(m) is the depth, h (m) is the maximum drainage path, $T_v$ (-) is the time factor and η is the electrode efficiency.

## 4.5 Degree of Consolidation and Settlement

The average degree of consolidation generated is essential to be calculated to evaluate the consolidation under the combined surcharge pressure, vacuum pressure and electroosmosis. It is expressed as,

$$U_{ave}(\%) = \frac{total\ volume\ change\ at\ time\ t}{ultimate\ total\ volume\ change} \times 100\%$$
$$= \frac{\int_0^H (u_i - u)dz}{\int_0^H (u_i - u_f)dz} = \frac{\int_0^{2h} qdz - \int_0^{2h} u_q dz - \int_0^h u_v dz - \int_0^h u_{ek} dz}{\int_0^{2h} (q - p_v)dz + \int_0^h \eta \frac{k_e}{k_h} \gamma_w U \frac{z}{h} dz} \quad [4.6]$$

Where $U_{ave}$ (-) is the average degree of consolidation, $u_i$ (kPa) is the initial excess pore water pressure, $u_f$ (kPa) is the final excess pore water pressure and u (kPa) is the excess pore water pressure expressed in Eq [4.5].

`

The derivation of the solution is in Appendix 1.

The settlement at a given time t can be calculated as,

$$s(t) = U_{ave}(\%) \cdot s_{ult} \qquad [4.7]$$

Where s(t) (m) is the settlement at a given time, $U_{ave}$ (-) is the average degree of consolidation and $s_{ult}$ (m) is the ultimate settlement expressed as,

$$s_{ult} = \sum_{i=1}^{\infty} \Delta h_i \frac{c_{ci}}{1+e_0} \log \frac{\sigma_0^{'} + q - p_v - u_f}{\sigma_0^{'} + q} \qquad [4.8]$$

Where $c_c$ [-] is the compression index $\sigma_0$' is the initial effective stress, q (kPa) is the surcharge loading, $p_v$ (kPa) is the vacuum pressure, $u_f$ (kPa) is the final excess pore water pressure, $e_0$ (-) is the initial void ratio and h (m) is the thickness of the layer.

## 4.6 Parameters

The compression index (Cc), hydraulic conductivity ($k_h$) and the coefficient of consolidation ($c_v$) are key variables in the model. Traditionally, these variables can be obtained from the standard oedometer test. However, it is difficult to perform the standard test in this study. Two reasons are attributed to this result. Firstly, the difficulty in measuring these properties of MFT in the standard test is due to the high compressibility and large void ratio (Proskin 1998). Secondly, the soil specimen cannot be completely trimmed for the standard test after the treatment because the diameter of the EK-vacuum cell is similar with that of the oedometer ring. Specifically, the diameters of the cell and the ring are 88mm and 50mm respectively.

`

The determination of these parameters in this study is illustrated in the following section.

### 4.6.1Compression Index

The compression index signifies the features of the relationship between the compressive stress and volume change (Gregory et al 2006). The compression index of clay reported in the literature is summarized in Table 4.1.It is typically in the range from 0.15 to 1. The compression index can be obtained from the standard oedometer test. It is the slope of the linear portion of e-log σ' curve (Craig 2004). However, the results of oedometer test can be misleading and the special oedometer test or field tests are needed when the compression index of soils is larger than 0.82, (Ulf et al 1999). Alternatively, physical properties such as the water content, plasticity index or void ratio can be used to estimate the compressibility index. This has been proposed by many researchers (Skempton and Jones 1944 and Wroth and Wood 1978).

In this thesis, the compression index is estimated from the correlation based on the experimental data of MFT (Ulf et al 1999 and Qiu and Sego 2001). The linear relationship between the compression index and void ratio with the empirical equation is presented in Fig 4.3,

$$c_c = 0.2014 \cdot e_0 - 0.0301 \qquad [4.9]$$

Where $e_0$ (-) is the initial void ratio and it is equal to 4.68.

`

The value of the compression index used in the model is 0.91 based on the correlation above. It falls into the range of the compression index of soft clay. This result, therefore, is plausible to be used in the theoretical analysis.

### 4.6.2 Hydraulic conductivity

The hydraulic conductivity can be obtained by indirect method (oedometer test or EK cell test (Elazar 2011), standard constant head or falling head test (Suthaker and Scott 1996). In this study, a series of falling head tests (ASTM D5856 2007) was carried out to measure the hydraulic conductivity of MFT-B. Before the test, samples were placed in the cell and consolidated to a given void ratio. The value of hydraulic conductivity used in the calculation is $2.55\times10^{-9} m/s$.

### 4.6.3 Coefficient of Consolidation

The coefficient of consolidation, $c_v$, is a vital parameter in the consolidation model. It can be expressed as,

$$c_v = \frac{k_h \cdot (1+e_0)}{m_v \gamma_w} \qquad [4.10]$$

Where $k_h$ (m/s) is the hydraulic conductivity, $e_0$ (4.68) is the initial void ratio, $\gamma_w$ (9.8 kN/m$^3$) is the unit weight of water and $m_v$ (m$^2$/kN) is the coefficient of volume compressibility. $m_v$ can be calculated by the equation below,

$$m_v = \frac{1}{1+e_0} \cdot \frac{e_0 - e_1}{\Delta\sigma} \qquad [4.11]$$

`

Where $e_0$ (4.68) is the initial void ratio, $e_1$ is the final void ratio (1.46 from EK cell test. See Table 3.3) and $\Delta\sigma$ is the increase in the effective stress.

In this study, the increase in the effective stress in the equation is summarized from published statistical data (Paul 2011). The consolidation data of seven samples of tailings recovered in Alberta is shown in Table 4.2. The data is in the terms of the void ratio and the effective stress. It can be concluded that when the void ratio decreases from around 4.86 to about 1.46, the average increase in the effective stress is about 40kPa.

Therefore,

$$m_v = \frac{1}{1+4.68} \cdot \frac{4.68-1.46}{40} = 0.014 m^2 / kN \qquad [4.12]$$

and

$$c_v = \frac{k_h \cdot (1+e_0)}{m_v \gamma_w} = \frac{2.55\times10^{-9} \times (1+4.68)}{0.014 \times 9.8} = 1.06\times10^{-7} m^2 / s \qquad [4.13]$$

## 4.7 Example and Discussion

The theoretical result is presented in this example based on the parameters obtained in E3V3 series (See Table 4.3 for input parameters). The surcharge loading in the model is set to be 0. In this example, the comparison is also made between the result of the theoretical model and the one obtained from the same E3V3 test series (the combination of 15 A/m$^2$ current density and 50kPa vacuum pressure). The result

`

is shown in Fig 4.4.

The ultimate settlement is,

$$
\begin{aligned}
s_u &= \sum_{i=1}^{\infty} \Delta h_i \frac{C_{ci}}{1+e_0} \log \frac{\sigma_0^{'} + q - p_v - u_f}{\sigma_0^{'} + q} \\
&= 6.5 \cdot \frac{0.91}{1+4.68} \cdot \log \frac{(14.8-9.8)\cdot 0.065 - (-100)}{(14.8-9.8)\cdot 0.065} \\
&= 2.61 cm
\end{aligned}
\qquad [4.14]
$$

As is shown in Fig.4.4, the model based on the small strain theory can reasonably predict the time rate of consolidation, i.e. $0.0075 \mathrm{cm/min}$. However, the discrepancies in the settlement between the model and experimental data in the E3V3 series can be observed. The settlement predicted by the model is 2.61 cm and it is around 40% of the total height of the sample. The result from the model is smaller than the measured value (4 cm), which is about 60% of the total height of the sample. This result is mainly attributed to the assumptions made in the model development. The discussion is as follows.

1) Soil is fully saturated and homogeneous. It is acceptable to regard that the soil is saturated and homogeneous because MFT is liquid-like and well blended.

2) The soil self-weight consolidation is negligible and the coefficient of consolidation ($c_v$) is constant during consolidation process. The assumption that hydraulic conductivity is constant and self-weight is negligible is the major cause of the gap between the results of the model and the tests. These assumptions are based on the small strain theory for incompressible soil properties (Ahmed and Siddiqua 2014).

`

However, the MFT has large void ratio and high compressibility. These properties lead to the significant changes of permeability with changing void ratio (Huerta and Rodriguez 1992). A theoretical model based on large strain consolidation for combined action of surcharge loading, vacuum pressure and EK treatment, therefore, is needed to interpret the consolidation of MFT.

3) The movement of solids induced by the hydraulic flow and electrophoresis is negligible. This assumption is on the basis of incompressible soil mass (Esrig 1968). However, the particle migration due to the hydraulic flow and electrophoresis may contribute to the changes in the void ratio of MFT.

4）Physical-chemical reactions generated by electrochemical reactions in soil and vicinity of electrodes are ignored. The reaction leads to the changes of the pH condition that affects the mobility of ions. The gases generated could also affect the efficiency of EK treatment.

5) The interaction of vacuum pressure and EK is not considered. The application of the vacuum pressure can remove gas bubbles generated near electrodes and the efficiency of EK treatment can be enhanced.

## 4.8 Summary

In this Chapter, an analytical model for one dimensional consolidation by surcharge loading, vacuum pressure and EK treatment was developed. The result was evaluated by the comparison with the experimental data reported in Chapter 3. The derivation of the model was based on the linear superposition of the surcharge loading,

`

vacuum pressure and electroosmotic consolidation. The results showed that the model predicted the consolidation rate well. However, a theoretical model based on large strain consolidation for combined action of surcharge loading, vacuum pressure and EK treatment was needed to accurately predict the settlement because of the nature of high compressibility of MFT.

`

Table 4.1 Summary of Compression Index for Different Kinds of Clay (Widodo and Ibrahim 2012).

| Type of soil | Compression index, Cc |
|---|---|
| Firm Clay | 0.03~0.06 |
| Stiff Clay | 0.06~0.15 |
| Soft Clay | 0.15~1.0 |

`

Table 4.2 Volume Compressibility Data in the Literature for Oil Sand Tailings (Modified from Paul 2011)

| Sample 1 (Miller et al., 2010a) | | Sample 2 (Miller et al., 2010a) | | Sample 3 (Miller et al., 2010a) | | Sample 4 (Miller et al., 2010a) | | Sample 5 (Miller et al., 2010a) | | Sample 6 (Lord and Liu, 1998) | | Sample 7 (Jeeravipoolvarn et al., 2008) | |
|---|---|---|---|---|---|---|---|---|---|---|---|---|---|
| Effective Stress (kPa) | Void Ratio | Effective Stress (kPa) | Void Ratio | Effective Stress (kPa) | Void Ratio | Effective Stress (kPa) | Void Ratio | Effective Stress (kPa) | Void Ratio | Effective Stress (kPa) | Void Ratio | Effective Stress (kPa) | Void Ratio |
| 0.02 | 7.8 | 0.02 | 7.51 | 0.02 | 7.56 | 0.02 | 7.56 | 0.02 | 7.58 | 0.38 | 5.14 | 0.092 | 4.91 |
| 0.04 | 6.79 | 0.03 | 6.91 | 0.04 | 6.68 | 0.04 | 6.68 | 0.04 | 6.67 | 1.51 | 2.94 | 0.96 | 3.38 |
| 0.08 | 5.65 | 0.05 | 6.05 | 0.08 | 5.58 | 0.08 | 5.58 | 0.1 | 5.21 | 2.61 | 2.52 | 3.42 | 2.7 |
| 0.15 | 4.83 | 0.1 | 4.72 | 0.14 | 4.88 | 0.14 | 4.88 | 0.3 | 4.11 | 5.04 | 2.22 | 6.84 | 2.38 |
| 0.35 | 3.91 | 0.3 | 3.35 | 0.3 | 3.96 | 0.3 | 3.96 | 0.7 | 3.45 | 10 | 1.95 | 9.85 | 2.05 |
| 0.6 | 3.49 | 0.6 | 2.79 | 0.6 | 3.34 | 0.6 | 3.26 | 2 | 2.98 | 20 | 1.72 | 26 | 1.78 |
| 1 | 3.14 | 2 | 2.23 | 2 | 2.67 | 2 | 2.67 | 5 | 2.49 | 40 | 1.48 | 78 | 1.54 |
| 2.5 | 2.72 | 6 | 1.86 | 5 | 2.18 | 5 | 2.18 | 10 | 2.26 | 80 | 1.32 | 92 | 1.38 |
| 5 | 2.33 | 10 | 1.74 | 10 | 1.79 | 10 | 1.79 | 20 | 2.04 | 170 | 1.21 | 255 | 1.22 |
| 10 | 2 | 20 | 1.58 | 20 | 1.51 | 20 | 1.51 | 40 | 1.76 | — | — | 450 | 1.03 |
| 20 | 1.79 | 40 | 1.4 | 40 | 1.29 | 40 | 1.29 | 80 | 1.32 | — | — | — | — |
| 40 | 1.49 | 80 | 1.21 | 80 | 1.13 | 80 | 1.13 | 40 | 1.49 | — | — | — | — |

`

Table 4.3 Example Input Information for Analytical Model

| parameters | Unit | value |
|---|---|---|
| Compression index Cc | — | 0.98 |
| Hydraulic conductivity, $k_h$ | m/s | $2.55\times10^{-9}$ |
| Coefficient of electroosmosis permeability, $k_e$ | $m^2/sV$ | $4.95\times10^{-9}$ |
| Coefficient of consolidation ,$c_v$ | $m^2/s$ | $1.06\times10^{-7}$ |
| Maximum voltage, $U_m$ | V | 15 |
| Vacuum pressure, $p_v$ | kPa | –50 |
| Surcharge loading, q | kPa | 0 |
| Sample height, h | M | 0.065 |

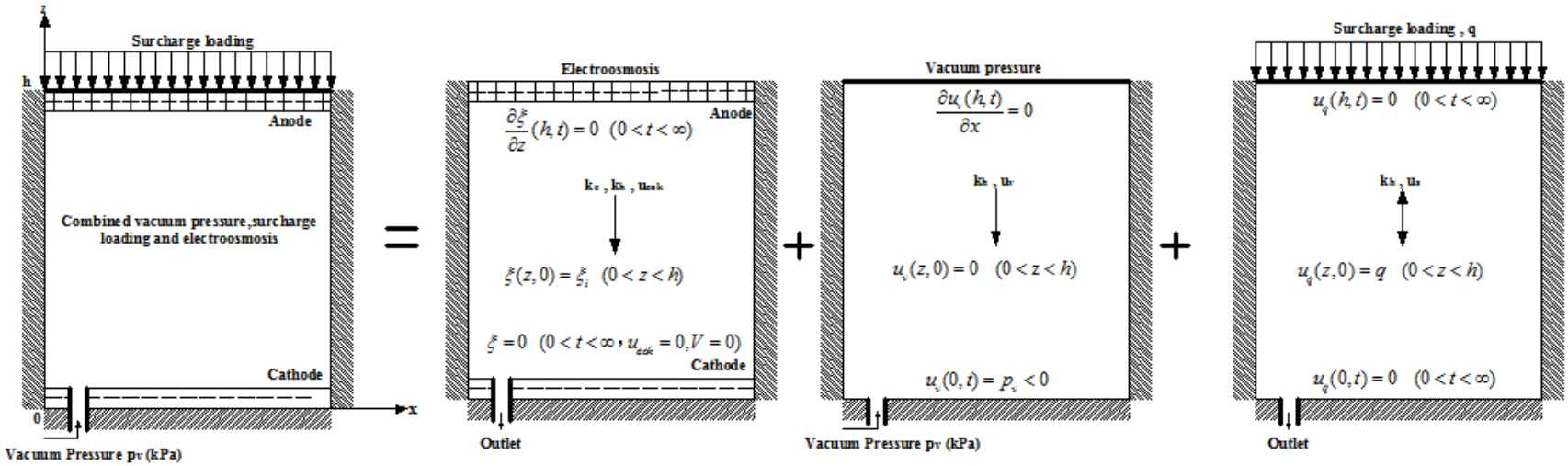


Fig 4.1 Analytical Model

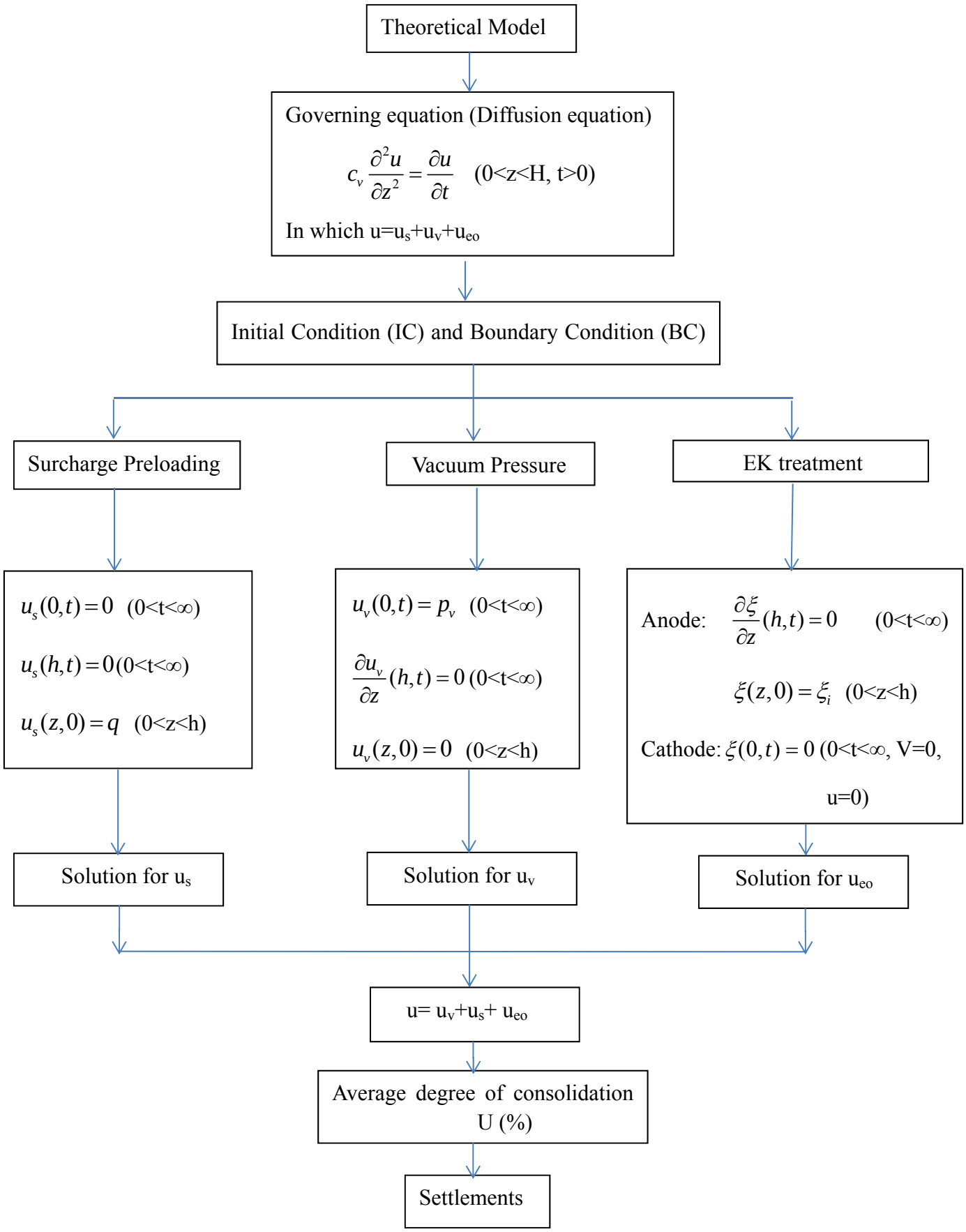


Fig 4.2 Flow Sheet of Model Structure

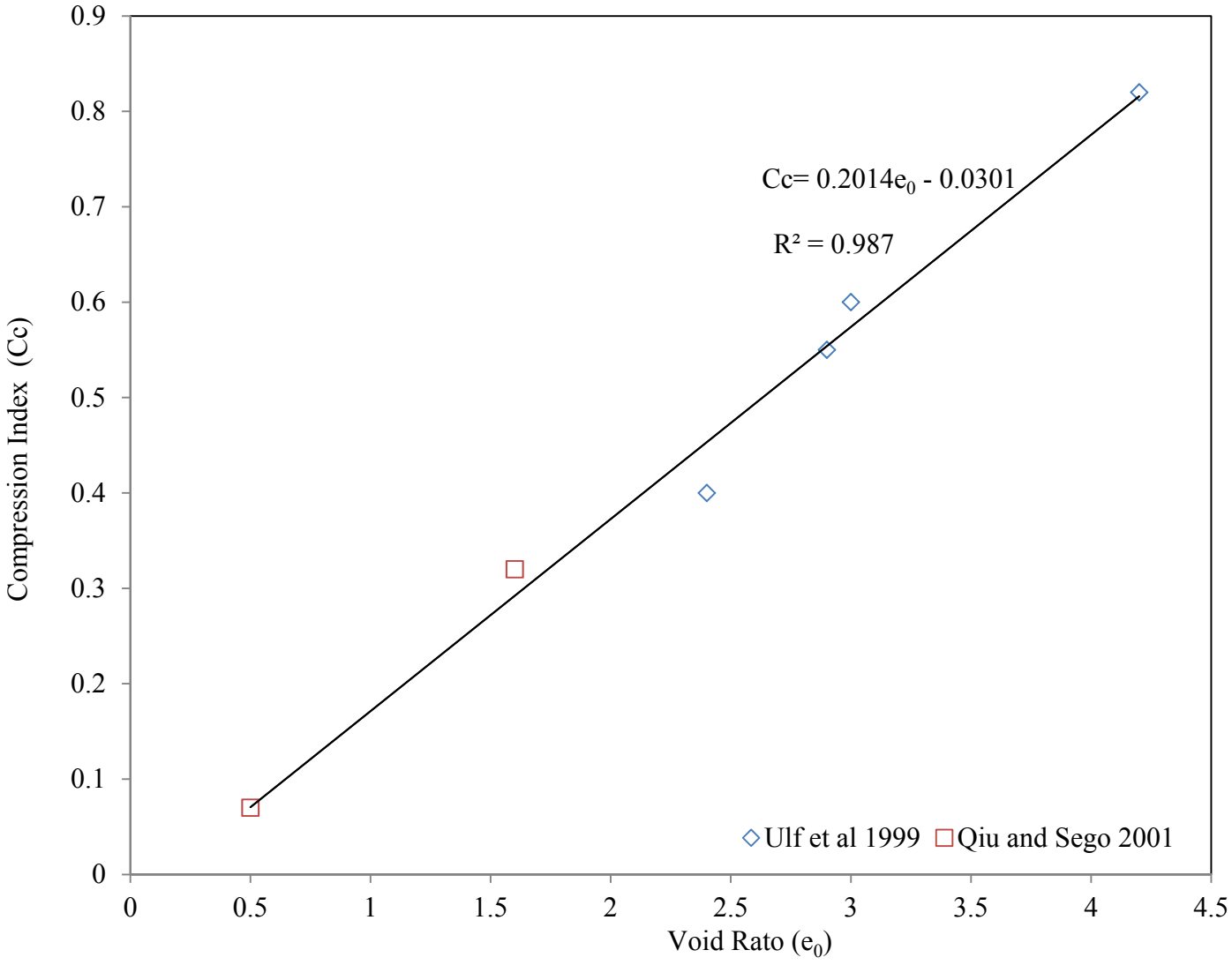


Fig 4.3 Correlation between Compression Index and Void Ratio of MFT

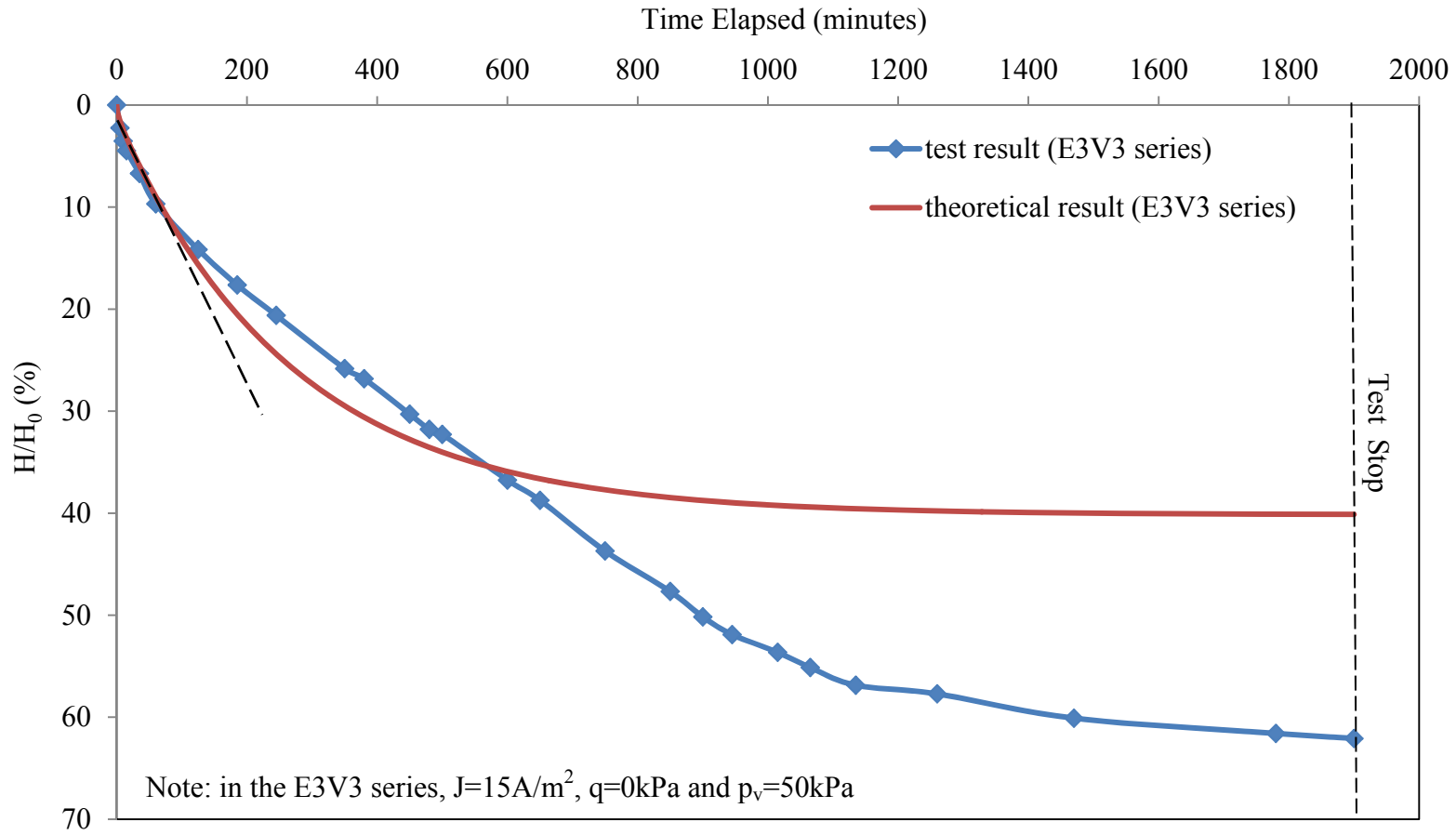


Fig 4.4 Theoretical and Experimental Normalized Settlement VS Time

`

# CHAPTER 5 CONCLUSION AND RECOMMENDATION FOR FUTURE RESEARCH

## 5.1 Summary

In this thesis, an experimental and theoretical analysis on EK and vacuum combined dewatering of MFT was studied. The physical and chemical properties of the MFT recovered from the northern Alberta were measured. The mineralogy and chemical composition of the MFT were classified. The coefficient of electroosmosis permeability was also measured to verify the feasibility of EK dewatering for the MFT.

An EK-vacuum cell was designed and manufactured to perform a series of tests with the combined action of EK, vacuum pressure and surcharge loading. The water discharged, settlement, undrained shear strength, water content, Atterberg limits and power consumption after the treatment were measured and in-depth analysis was made. One dimensional consolidation model considering the influence of EK, vacuum pressure and surcharge loading was developed to simulate the consolidation behavior of MFT. The model was verified by the comparison with the results from experiments.

## 5.2 Conclusions

The conclusion of this thesis can be made as following.

- The MFT recovered from northern Alberta was fluid-like with water content 188%

`

± 2%, specific gravity 2.49, initial void ratio 4.68, organic matter 19.9%, and low carbonate content (< 1%). The main minerals included illite, kaolinite and quartz.

- The measured EO permeability in the EK cell test was from $2.77 \times 10^{-9}$ $m^2/sV$ to $4.95 \times 10^{-9}$ $m^2/sV$. It indicated the feasibility of EK treatment on the MFT.

- The EK and vacuum combined dewatering process (EV series) was the most effective in decreasing the water content and enhancing the undrained shear strength. The undrained shear strength after the treatment in the EV series exceeded 5kPa and the final settlement could reach 50% to 60% of the total height of the sample.

- The final water content decreased linearly with the increasing current density and vacuum pressure. On the other hand, the final undrained shear strength increased linearly with the increasing current density and the vacuum pressure.

- In the EK and vacuum combined treatment, EK was in the dominant position in dewatering and strength gain.

- The plastic index of the MFT increased after the EK treatment. It was mainly attributed to the increase in the liquid limit.

- In the EV series, the increase in the vacuum pressure resulted in the increase in the power consumption for EK treatment under the constant current density.

- The consolidation rate of 0.0075cm/min from the model for one dimensional

`

consolidation by surcharge loading, vacuum pressure and EK treatment was consistent with that from the tests. However, the model could not predict the consolidation settlement properly. It was mainly due to the high compressibility of MFT. A large strain consolidation model was needed for the prediction of volume change and settlement of MFT.

## 5.3 Recommendations

Recommendations for the future study include:

- Develop a large scale pilot test apparatus
- Develop a large strain consolidation model for the combined action of EK, vacuum and surcharge loading.
- Develop a two dimensional model to facilitate in-situ applications.
- Design and implement a field test on the dewatering of MFT in a tailings storage facility.

`

# BIBLIOGRAPHY

**Ahmed, S. I., & Siddiqua, S. (2014).** A review on consolidation behavior of tailings. International Journal of Geotechnical Engineering, 8(1), 102-111.

**Alberta Energy Regulator (2015)** Tailings Management Framework for Mineable Athabasca Oil Sands (TMF). Obtained from: http://aep.alberta.ca/lands-forests/ cumulative-effects/regional-planning/documents/LARP-TailingsMgtAthabascaOilsands-Mar2015.pdf.

**Alberta Energy (2015).** PDF Map of Alberta's Oil Sands Leased Area. Obtained from: http://www.energy.alberta.ca/LandAccess/pdfs/OSAagreeStats.pdf

**Alberta Energy (2014).** Facts and Statics. Obtained from: http://www. energy. alberta.ca/oilsands/ 791.asp

**Allen, E. W. (2008).** Process water treatment in Canada's oil sands industry: I. Target pollutants and treatment objectives. Journal of Environmental Engineering and Science, 7(2), 123-138.

**Asadi, A., Huat, B. B., Nahazanan, H., and Keykhah, H. A. (2013).** Theory of electroosmosis in soil. International Journal of Electrochemical Science,8(1), 1016-1025.

**ASTM D2974-14 (2015).** Standard test methods for moisture, ash, and organic matter of peat and other organic soils. ASTM International, West Conshohocken, PA, DOI:

`

10.1520/D2974-14.

**ASTM Standard D4318 (2010).** Standard test methods for liquid limit, plastic limit, and plasticity index of soils. ASTM International, West Conshohocken, PA, DOI: 10.1520/ D4318-10

**ASTM Standard D5856 (2007).** Standard test method for measurement of hydraulic conductivity of porous material using a rigid-wall, compaction-mold permeameter. ASTM International, West Conshohocken, PA, DOI: 10.1520/D5856-95R07.

**Basack, S. (2011)** A review of the use of the preloading technique and vertical drains for soil consolidation. Proceedings of Indian Geotechnical Conference, Kochi. No. H-029, 361-364.

**BGC Engineering Inc. (2010).** Oil sands tailings technology review. Oil Sands Research and Information Network, University of Alberta, School of Energy and the Environment, Edmonton, Alberta. OSRIN Report No. TR-1.

**Bourgès-Gastaud, S., Stoltz, G., Dolez, P., Blond, É., and Touze-Foltz, N. (2014).** Laboratory device to characterize electrokinetic geocomposites for fluid fine tailings dewatering. Canadian Geotechnical Journal, 52(4), 505-514.

**Brown, D.C. (2013).** MSc thesis: Calcium nitrate treatment of oil sand tailings for improved densification and reduced greenhouse gas emissions. University of Calgary, Calgary, Alberta, Canada.

**Brown, D., Ramos-Padrón, E., Gieg, L., and Voordouw, G. (2013).** Effect of

`

calcium ions and anaerobic microbial activity on sedimentation of oil sands tailings. International Biodeterioration & Biodegradation, 81, 9-16.

**Cabrera, S. C. M. (2008).** Doctoral dissertation：Characterization of Oil Sands Tailings Using Low Field Nuclear Magnetic Resonance (NMR) Technique , University of Calgary, Calgary, Alberta, Canada.

**CasagrandeL.,(1952)** Electro-osmotic stabilization of soils. Journal of the Boston Society of Civil Engineers, 39 (1), 285-317.

**Chai, J. C., and Carter, J. P. (2013).** Consolidation theory for combined vacuum pressure and surcharge loading. In Proceedings of the 18th International Conference on Soil Mechanics and Geotechnical Engineering, Paris, 2449-2452

**Chew, S. H., Karunaratne, G. P., Kuma, V. M., Lim, L. H., Toh, M. L., and Hee, A. M. (2004).** A field trial for soft clay consolidation using electric vertical drains. Geotextiles and Geomembranes, 22(1), 17-35.

**Chu, J., Yan, S., and Indraranata, B. (2008).** Vacuum preloading techniques-recent developments and applications. GeoCongress, New Orleans, Geosustainability and Geohazard Mitigation GPS 178, Reddy, KR, Khire, MV, Alshawabkeh, AN (eds), 586-595.

**Craig, R. F. (2004).** Craig's soil mechanics, seventh edition. CRC Press.

**Dawson, R.F., Sego, D.C., and Pollock, G.W. (1999).** Freeze-thaw dewatering of oil

`

sands fine tails. Canadian Geotechnical Journal, 36 (4), 587-598.

**Dreimanis, A. (1962).** Quantitative gasometric determination of calcite and dolomite by using Chittick apparatus. Journal of Sedimentary Research,.32 (3). 520-529

**Dunbar, R. B., and Eng, P. (2007).** Canada's Oil Sands-A World-Scale Hydrocarbon Resource. Strategy West Inc. Calgary, Alberta, Canada. Obtained from: http://www.strategywest.com/downloads/StratWest_OilSands.pdf

**Elazar, R. (2011).** MESc thesis: Electrokinetic dewatering of orr dam sediment. University of Western Ontario, London, Ontario, Canada.

**Esrig, M. I. (1968).** Pore pressures, consolidation, and electrokinetics. Journal of the Soil Mechanics and Foundations Division, 94(4), 899-922.

**Gopalakrishnan, S., Mujumdar, A. S., Weber, M. E., and Pirkonen, P. M. (1996).** Electrokinetically enhanced vacuum dewatering of mineral slurries.Filtration & separation, 33(10), 929-932.

**Gregory, A. S., Whalley, W. R., Watts, C. W., Bird, N. R. A., Hallett, P. D., and Whitmore, A. P. (2006).** Calculation of the compression index and precompression stress from soil compression test data. Soil and Tillage Research, 89(1), 45-57.

**Griffin, H., and O'Kelly, B. C. (2014).** Ground improvement by vacuum consolidation–a review. Proceedings of the Institution of Civil Engineers-Ground Improvement, 167(4), 274-290.

`

**Guo, Y., and Shang, J. Q. (2014).** A study on electrokinetic dewatering of oil sands tailings. Environmental Geotechnics, 1(2), 121-134.

**Hande Aharnish Bhojaraj (2014)** Doctoral dissertation: Accelerated Dewatering and Drying Treatment of Oil Sands Tailings by Electrical Resonant Auto-Transformer. University of Alberta, Edmonton, Alberta, Canada.

**Holtz, R. D., and Kovacs, W. D. (1981).** An introduction to geotechnical engineering. Prentice Hall, Englewood Cliffs, New Jersey, USA.

**Huerta, A., and Rodriguez, A. (1992).** Numerical analysis of non-linear large-strain consolidation and filling. Computers & Structures, 44(1), 357-365.

**Indraratna, B., Chu, J., and Hudson, J. A. (2005).** Ground Improvement: Case Histories. Oxford, UK: Elsevier.

**Islam, S. (2014).** MESc thesis: Thickening of Mature Fine Oil Sands Tailings University of Western Ontario, London, Ontario, Canada.

**Jeeravipoolvarn, S. (2010).** Doctoral dissertation: Geotechnical behavior of in-line thickened oil sands tailings. University of Alberta, Edmonton, Alberta, Canada.

**Johnson, R.L., Bork, P., Allen, E.A.D., James, W.H., and Koverny, L. (1993).** Oil sands sludge dewatering by freeze-thaw and evapotranspiration. Alberta LandConservation and Reclamation Council, Reclamation Research Technical Advisory Committee. Report No. RRTAC 93-8.

`

**Lee, M (2000).** Doctoral dissertation: An experimental and analytical study of electrokinetic consolidation. University of Oxford, Oxford, England, United Kingdom.

**Liu, H. L., Cui, Y. L., Shen, Y., and Ding, X. M. (2014).** A new method of combination of electroosmosis, vacuum and surcharge preloading for soft ground improvement. China Ocean Engineering, 28, 511-528.

**Lockhart, N. C. (1983).** Electroosmotic dewatering of clays, III. Influence of clay type, exchangeable cations, and electrode materials. Colloids and Surfaces, 6(3), 253-269.

**Lo, K. Y., Ho, K. S., and Inculet, I. I. (1991).** Field test of electroosmotic strengthening of soft sensitive clay. Canadian Geotechnical Journal, 28(1), 74-83.

**MacKinnon, M. D., and Boerger, H. (1986).** Description of two treatment methods for detoxifying oil sands tailings pond water. Water quality research journal of Canada, 21(4), 496-512.

**Mahfouz, A. H. (2013).** Vacuum preloading combined electroosmotic strengthening of ultra-soft soil. Journal of Central South University, 20(11), 3282-3295.

**Masse, F., Spaulding, C. A., Wong, I. C., and Varaksin, S. (2001, June).** Vacuum consolidation: A review of 12 years of successful development. In Proceedings of the GeoOdyssey 2001 Conference. Virginia Polytechnic Institute and State University,

`

Blacksburg, Virginia, USA, 1–23.

**McMartin, D. W. (2003).** Doctoral dissertation: Persistence and fate of acidic hydrocarbons in aquatic environments: naphthenic acids and resin acids. University of Saskatchewan, Saskatoon, Saskatchewan, Canada.

**Micic, S., Shang, J. Q., Lo, K. Y., Lee, Y. N., and Lee, S. W. (2001).** Electrokinetic strengthening of a marine sediment using intermittent current. Canadian Geotechnical Journal, 38(2), 287-302.

**Mohamedelhassan, E. (2002).** Doctoral dissertation: Soil improvement using electrokinetic and vacuum techniques. University of Western Ontario, London, Ontario, Canada.

**Mok, C. K. (2006).** Doctoral dissertation: Design and modelling of electroosmotic dewatering. University of Newcastle upon Tyne, England, UK.

**Onyelowe Ken, C., and Okoafor, F. O. (2012).** Geochemistry of soil stabilization. ARPN Journal of Earth Sciences, 1(1), 32-35

**Owolagba, J. O. (2013).** Doctoral dissertation: Dewatering Behavior of Centrifuged Oil Sand Fine Tailings for Surface Deposition. University of Regina, Regina, Saskatchewan, Canada.

**Paul, A. C. (2011).** Doctoral dissertation: Statistical modeling for tailings consolidation using index properties. University of Regina, Regina,

`

Saskatchewan, Canada.

**Priscu, C (1999).** Doctoral dissertation: Behavior of mine tailings dams under high tailings deposition rates. McGill University, Montreal, Canada.

**Proskin, S.A. (1998).** Doctoral dissertation: A geotechnical investigation of freeze-thaw dewatering of oil sands fine tailings. University of Alberta, Edmonton, Alberta, Canada.

**Qiu, Y., and Sego, D. C. (2001).** Laboratory properties of mine tailings. Canadian Geotechnical Journal, 38(1), 183-190.

**Robinson, R. G., Indraratna, B., and Rujikiatkamjorn, C. (2012).** Final state of soils under vacuum preloading. Canadian Geotechnical Journal, 49(6), 729-739.

**Rowe, R.K. (2001).** Geotechnical and Geoenvironmental Engineering Handbook. Kluwer Academic Publishing, Norwell, MA, USA.

**Rujikiatkamjorn, C., Indraratna, B., and Chu, J. (2007).** Numerical modelling of soft soil stabilized by vertical drains, combining surcharge and vacuum preloading for a storage yard. Canadian Geotechnical Journal, 44(3), 326-342.

**Saowapakpiboon, J., Bergado, D. T., Voottipruex, P., Lam, L. G., and Nakakuma, K. (2011).** PVD improvement combined with surcharge and vacuum preloading including simulations. Geotextiles and Geomembranes, 29(1), 74-82.

**Sennett, P., and Olivier, J. P. (1965).** Colloidal dispersions, electrokinetic effects, and

`

the concept of zeta potential. Industrial & Engineering Chemistry, 57(8), 32-50.

**Shang, J. Q., Tang, M., and Miao, Z. (1998).** Vacuum preloading consolidation of reclaimed land: a case study. Canadian Geotechnical Journal, 35(5), 740-749.

**Shang, J. Q. (1998).** Electroosmosis-enhanced preloading consolidation via vertical drains. Canadian Geotechnical Journal, 35(3), 491-499.

**Shang, J. Q., and Lo, K. Y. (1997).** Electrokinetic dewatering of a phosphate clay. Journal of Hazardous Materials, 55(1), 117-133.

**Shang, J.Q, Lo, K. Y., and Quigley, R. M. (1994).** Quantitative determination of potential distribution in Stern-Gouy double-layer model. Canadian Geotechnical Journal, 31(5), 624-636

**Skempton, A. W., and Jones, O. T. (1944).** Notes on the compressibility of clays. Quarterly Journal of the Geological Society, 100(1-4), 119-135.

**Smollen, M., and Kafaar, A. (1994).** Electroosmotically enhanced sludge dewatering-pilot-plant study.Water Sci. Technol. 30(8),159-168

**Soga, K., and Mitchell, J. K. (2005).** Fundamentals of soil Behavior, third Edition. John Wiley and Sons, Inc.

**Sparks, D. L. (Ed.). (1998).** Soil physical chemistry. CRC press.

`

**Suthaker, N. N., and Scott, J. D. (1996).** Measurement of hydraulic conductivity in oil sand tailings slurries. Canadian geotechnical journal, 33(4), 642-653.

**Tang, M., and Shang, J. Q. (2001).** Vacuum preloading consolidation of Yaoqiang Airport runway; Soil improvement by the vacuum preloading method for an oil storage station; Consolidation of a very soft clay with vertical drains. Géotechnique, 52(2), 148-154.

**Torghabeh, E. A. (2013).** Doctoral dissertation: Stabilization of Oil Sands Tailings Using Vacuum Consolidation .University of Alberta, Edmonton, Alberta, Canada

**Ulf Barnekow, Matthias Haase and Christoph Wels (1999)** Geomechanical fine tailings characterization and 1D-consolidation modeling of Slime Zones at WISMUT Tailings Impoundments. Soft Tailings Stabilization Workshop. Part II: Practice and Experiences. Chemnitz, Germany. Obtained from: http://www.infomine.com/library/ publications/docs/barnekow.pdf.

**Widodo, S., and Ibrahim, A. (2012).** Estimation of primary compression index (CC) using physical properties of Pontianak soft clay. International Journal of Engineering Research and Applications (IJERA), 2(5), 2232-2236.

**Wroth, C. P., and Wood, D. M. (1978).** The correlation of index properties with some basic engineering properties of soils. Canadian Geotechnical Journal,15(2), 137-145.

`

**Yan, H. S., and Cao, D. Z. (2005).** Application of low-level vacuum preloading technique in offshore projects. Ocean and River Hydraulics, 3, 41-43.

**Yan, S. W., and Chu, J. (2005).** Soil improvement for a storage yard using the combined vacuum and fill preloading method. Canadian Geotechnical Journal, 42(4), 1094-1104.

`

# APPENDIX

## Derivation for the Analytical 1D Consolidation EVS Model

In the upper expression,

$$\int_0^{2h} q\,dz = 2hq \qquad \text{[A-1]}$$

$$\begin{aligned}
\int_0^{2h} u_q\,dz &= \int_0^{2h} q\sum_{n=0}^{\infty}\left(\frac{4}{(2n+1)\pi}\sin\frac{(2n+1)\pi z}{2h}\right)\exp\left(-\frac{(2n+1)^2\pi^2 T_v}{4}\right)dz \\
&= q\sum_{n=0}^{\infty}\left(\frac{4}{(2n+1)\pi}\exp\left(-\frac{(2n+1)^2\pi^2 T_v}{4}\right)\frac{2h}{(2n+1)\pi}(-1)\cos\left(\frac{2n+1}{2h}\pi z\right)\right|_0^{2h} \\
&= q\sum_{n=0}^{\infty}\left(\frac{8h}{(2n+1)^2\pi^2}\exp\left(-\frac{(2n+1)^2\pi^2 T_v}{4}\right)(-1)(-1-1)\right. \\
&= q\sum_{n=0}^{\infty}\left(\frac{16h}{(2n+1)^2\pi^2}\exp\left(-\frac{(2n+1)^2\pi^2 T_v}{4}\right)\right.
\end{aligned} \qquad \text{[A-2]}$$

$$\begin{aligned}
\int_0^{h} u_v\,dz &= \int_0^{h} p_v\{1-\sum_{n=0}^{\infty}\left(\frac{4}{(2n+1)\pi}\sin\frac{(2n+1)\pi z}{2h}\right)\exp\left(-\left(\frac{2n+1}{2}\right)^2\pi^2 T_v\right)\}dz \\
&= hp_v - p_v\int_0^{h}\sum_{n=0}^{\infty}\left(\frac{4}{(2n+1)\pi}\sin\frac{(2n+1)\pi z}{2h}\right)\exp\left(-\left(\frac{2n+1}{2}\right)^2\pi^2 T_v\right)\}dz \\
&= hp_v - p_v\sum_{n=0}^{\infty}\left(\frac{4}{(2n+1)\pi}\exp\left(-\frac{(2n+1)^2\pi^2 T_v}{4}\right)\frac{2h}{(2n+1)\pi}(-1)\cos\left(\frac{2n+1}{2h}\pi z\right)\right|_0^{h} \\
&= hp_v - p_v\sum_{n=0}^{\infty}\left(\frac{8h}{(2n+1)^2\pi^2}\exp\left(-\frac{(2n+1)^2\pi^2 T_v}{4}\right)(-1)(0-1)\right. \\
&= hp_v - p_v\sum_{n=0}^{\infty}\left(\frac{8h}{(2n+1)^2\pi^2}\exp\left(-\frac{(2n+1)^2\pi^2 T_v}{4}\right)\right.
\end{aligned} \qquad \text{[A-3]}$$

`

$$\int_0^h u_{ek}dz = \int_0^h \{-\eta\frac{k_e}{k}\gamma_w V(x) + \eta\frac{2k_e\gamma_w V_m}{k\pi^2}\sum_{n=0}^{\infty}\frac{(-1)^n}{(n+\frac{1}{2})^2}\sin\frac{(n+\frac{1}{2})\pi z}{h}\exp[-(n+\frac{1}{2})^2\pi^2 T_v]\}dz$$

$$= -\eta\frac{k_e V_m}{k}\gamma_w\int_0^h\frac{z}{h}dz + \eta\frac{2k_e\gamma_w V_m}{k\pi^2}\int_0^h\sum_{n=0}^{\infty}\frac{(-1)^n}{(n+\frac{1}{2})^2}\sin\frac{(n+\frac{1}{2})\pi z}{h}\exp(-(n+\frac{1}{2})^2\pi^2 T_v)dz$$

$$= -\eta\frac{k_e V_m}{2k}\gamma_w h + \eta\frac{2k_e\gamma_w V_m}{k\pi^2}\sum_{n=0}^{\infty}\frac{(-1)^n}{(n+\frac{1}{2})^2}\frac{h}{(n+\frac{1}{2})\pi}\exp(-(n+\frac{1}{2})^2\pi^2 T_v)(-1)\cos\frac{(n+\frac{1}{2})\pi z}{h}\Big|_0^h$$

$$= -\eta\frac{k_e V_m}{2k}\gamma_w h + \eta\frac{2k_e\gamma_w V_m}{k\pi^2}\sum_{n=0}^{\infty}\frac{(-1)^n h}{(n+\frac{1}{2})^3\pi}\exp(-(n+\frac{1}{2})^2\pi^2 T_v)(-1)(0-1)$$

$$= -\eta\frac{k_e V_m}{2k}\gamma_w h + \eta\frac{16k_e\gamma_w V_m h}{k\pi^2}\sum_{n=0}^{\infty}\frac{(-1)^n}{(2n+1)^3\pi}\exp(-\frac{(2n+1)^2\pi^2 T_v}{4}) \qquad \text{[A-4]}$$

In the lower expression,

$$\int_0^{2h} qdz - \int_0^h p_v dz + \int_0^h \eta\frac{k_e}{k_h}\gamma_w V_m\frac{z}{h}dz = 2qh - hp_v + \eta\frac{k_e}{k_h}\gamma_w V_m\frac{1}{2}h \qquad \text{[A-5]}$$

Therefore,

$$U_{ave}(\%) = \frac{1}{2qh - hp_v + \eta\frac{k_e}{k_h}\gamma_w V_m\frac{1}{2}h}[2qh - qh\sum_{n=0}^{\infty}(\frac{16}{(2n+1)^2\pi^2}\exp(-\frac{(2n+1)^2\pi^2 T_v}{4}) - hp_v$$
$$+ p_v h\sum_{n=0}^{\infty}(\frac{8}{(2n+1)^2\pi^2}\exp(-\frac{(2n+1)^2\pi^2 T_v}{4}) + \eta\frac{k_e V_m}{2k_h}\gamma_w h -$$
$$\eta\frac{16k_e\gamma_w V_m h}{k_h\pi^2}\sum_{n=0}^{\infty}\frac{(-1)^n}{(2n+1)^3\pi}\exp(-\frac{(2n+1)^2\pi^2 T_v}{4}) \qquad \text{[A-6]}$$

`

# VITAE

**NAME:** Rui Zhang

**EDUCATION:** 2014 – present M.E.Sc.,

Department of Civil and Environmental Engineering, Faculty of Engineering, The University of Western Ontario

2008 – 2012 B.E.,

Department of Civil Engineering, Hunan University

**EMPLOYEMENT:** 2015.1-2016.4 Teaching Assistant,

Department of Civil and Environmental Engineering, Faculty of Engineering, The University of Western Ontario

2014.8-2014.12 Research Assistant,

Department of Civil and Environmental Engineering, Faculty of Engineering, The University of Western Ontario

2012.7-2013.12 Junior Engineer,

China Huanqiu Contracting &Engineering Corporation (SH), Shanghai, China

**AWARDS:** 2015 The R.M.Quigley Award